Long-Term Monitoring of Methane in New York State:

Assessing the Impact of Shifting Energy Portfolios on Regional Air Quality and Climate

Final Report | Report Number 23-21 | April 2020

NEW YORK STATE | NYSERDA

NYSERDA's Promise to New Yorkers:

NYSERDA provides resources, expertise, and objective information so New Yorkers can make confident, informed energy decisions.

Our Vision:

New York is a global climate leader building a healthier future with thriving communities; homes and businesses powered by clean energy; and economic opportunities accessible to all New Yorkers.

Our Mission:

Advance clean energy innovation and investments to combat climate change, improving the health, resiliency, and prosperity of New Yorkers and delivering benefits equitably to all.

Long-Term Monitoring of Methane in New York State:

Assessing the Impact of Shifting Energy Portfolios on Regional Air Quality and Climate

Final Report

Prepared for:

New York State Energy Research and Development Authority

Albany, NY

Ellen Burkhard, Ph.D.
Senior Advisor, Environmental Research

Prepared by:

University of Rochester, Department of Earth and Environmental Sciences

Rochester, NY

Lee T. Murray, Ph.D.
Assistant Professor

and

State University of New York Plattsburgh Center for Earth and Environmental Science

Plattsburgh, NY

Eric M. Leibensperger, Ph.D.
Associate Professor

NYSERDA Report 23-21 NYSERDA Contract 100413 April 2020

Notice

This report was prepared by the University of Rochester and the State University of New York Plattsburgh in the course of performing work contracted for and sponsored by the New York State Energy Research and Development Authority (hereafter "NYSERDA"). The opinions expressed in this report do not necessarily reflect those of NYSERDA or the State of New York, and reference to any specific product, service, process, or method does not constitute an implied or expressed recommendation or endorsement of it. Further, NYSERDA, the State of New York, and the contractor make no warranties or representations, expressed or implied, as to the fitness for particular purpose or merchantability of any product, apparatus, or service, or the usefulness, completeness, or accuracy of any processes, methods, or other information contained, described, disclosed, or referred to in this report. NYSERDA, the State of New York, and the contractor make no representation that the use of any product, apparatus, process, method, or other information will not infringe privately owned rights and will assume no liability for any loss, injury, or damage resulting from, or occurring in connection with, the use of information contained, described, disclosed, or referred to in this report.

NYSERDA makes every effort to provide accurate information about copyright owners and related matters in the reports we publish. Contractors are responsible for determining and satisfying copyright or other use restrictions regarding the content of reports that they write, in compliance with NYSERDA's policies and federal law. If you are the copyright owner and believe a NYSERDA report has not properly attributed your work to you or has used it without permission, please email print@nyserda.ny.gov

Information contained in this document, such as web page addresses, are current at the time of publication.

Abstract

This report describes a new observational network of high-quality continuous measurements of the greenhouse gas methane (CH_4) in New York State and its first application in a top-down inverse model framework to provide observational constraints on emissions of methane from New York State.

Keywords

Methane; Carbon Dioxide; Greenhouse Gas; Emission Estimate; Top-Down Constraint

Acknowledgments

This work was supported by NYSERDA Agreement No. 100413 and the University of Rochester.

Table of Contents

List of Figures

List of Tables

Acronyms and Abbreviations

ACT AMERICA	Atmospheric Carbon & Transport-America
AMoN	Ammonia Monitoring Network
APEI	Air Pollutant Emission Inventory
AQS	Air Quality System
ASRC	Atmospheric Sciences Research Center
CASTNet	Clean Air Status and Trends Network
CRDS	cavity ring-down spectrometry
CSN	Chemical Speciation Network
CTM	chemistry-transport model
DEC	Department of Environmental Conservation
DOT	Department of Transportation
ECCC	Environment and Climate Change Canada
EDGAR	Emissions Database for Global Atmospheric Research
EIA	Energy Information Administration
EIS	Environmental Impact Study
EPA	Environmental Protection Agency
ESA	European Space Agency
GEOS	Goddard Earth Observing System
GEPA	Gridded Environmental Protection Agency
GHGI	Greenhouse Gas Inventory
GMAO	Global Modeling and Assimilation Office
GMD	Global Monitoring Division
ICOS	Integrated Carbon Observation System
magl	meters above ground level
masl	meters above sea level
$MMtCO_2e$	million metric tons of CO_2 equivalent
NAAQS	National Ambient Air Quality Standards
MDA8	maximum daily 8-hour average
MDN	Mercury Deposition Network
MRP	Methane Reduction Plan
MSA	metropolitan statistical area
NADP	National Atmospheric Deposition Program
NASA	National Aeronautics and Space Administration
NATTS	National Air Toxics Trends Station
NCore	National Core
NEI2011	National Emissions Inventory version 2011
NEUS	Northeastern United States

NIST	National Institute of Standards and Technology
NMVOC	non-methane volatile organic compounds
NPMS	National Pipeline Mapping System
NTN	National Trends Network
NOAA	National Oceanic and Atmospheric Administration
NO_x	reactive nitrogen oxides
NYS	New York State
NYSERDA	New York State Energy and Research Development Authority
O&G	Oil and Gas
PCA	principal components analysis
ppbv	parts per billion by volume (≡ 1 nmol mol−1)
PHMSA	Pipeline and Hazardous Materials Safety Administration
PM	particulate matter
ppmv	parts per million by volume (≡ 1 μmol mol−1)
PSP	Pinnacle State Park
QA/QC	quality assurance/quality control
QFED	Quick Fire Emissions Database
RG&E	Rochester Gas & Electric
REV	Reforming the Energy Vision
ROC	Rochester
STILT	Stochastic Time-Inverted Lagrangian Transport Model
TROPOMI	TROPOspheric Monitoring Instrument
UPS	Uninterrupted Power Supply
USGS	United States Geological Survey
VOC	volatile organic compound
WHT	Whiteface Mountain Base
WMO	World Meteorological Organization

Executive Summary

The primary objective of this project was to establish high-quality continuous measurements of methane (CH_4) in New York State's ambient surface air and apply those measurements to the GEOS-Chem chemistry-transport model (CTM). The purpose of the project was to optimally constrain the spatial and temporal distribution of anthropogenic methane emissions from NYS and upwind regions and explore the downwind impacts.

Three Picarro G3201 cavity ring-down spectrometry (CRDS) analyzers measuring methane and carbon dioxide (CO_2) calibrated to National Oceanic and Atmospheric Administration (NOAA) reference standards have been deployed in continuous operation at three existing Department of Environmental Conservation (DEC) air-quality monitoring sites. Two rural sites (Pinnacle State Park in southwestern NY and Whiteface Mountain in northern NY) have been operational since October 2017, and one urban site has been operational since April 2018 (Rochester). The data has been quality-controlled for October 2017 through April 2020.

We assimilate the first full year of measurements contemporaneous with the European Space Agency (ESA) TROPOspheric Monitoring Instrument (TROPOMI) satellite instrument, as well as 22 neighboring monitoring sites and one aircraft campaign within the GEOS-Chem adjoint model. The assimilation generates a gridded emissions inventory for the Northeastern United States (NEUS) domain. Total emissions over NYS (natural and anthropogenic) increased by 2% relative to the baseline Gridded Environmental Protection Agency (GEPA) anthropogenic and WetCHARTs natural methane inventories for an annual total of 26.5 million metric tons of CO_2 equivalent ($MMtCO_2e$) over the period May 2018 to April 2019. Our constraints imply that the greatest in-State methane emissions exist in Western New York, the Finger Lakes, New York City, and Long Island. Our results are generally consistent with the bottom-up anthropogenic NYS Greenhouse Gas Inventory (GHGI), although that inventory has higher landfill emissions and the inventory developed for this report implies higher livestock emissions.

Full regional air-quality simulations using the GEOS-Chem CTM indicate that upwind non-methane volatile organic compound (NMVOC) emissions associated with unconventional Oil and Gas (O&G) extraction in the Marcellus Formation have minimal impact on surface ozone air quality in NYS.

1 Background and Motivation

Methane is the most abundant volatile organic compound (VOC) in the atmosphere, with an atmospheric lifetime of about nine years and a global warming potential about 30 times greater than that of carbon dioxide (CO_2) over 100-year time horizons. It is a major precursor for the production of tropospheric ozone, a criteria pollutant under the United States National Ambient Air Quality Standards (NAAQS) and also a potent greenhouse gas. Despite this, methane has long remained unregulated, and atmospheric abundances have tripled since the Industrial Revolution (Figure 1, resulting in 40% of all anthropogenic greenhouse-gas warming (IPCC, 2013) and a 5 parts per billion by volume ($\equiv$ 1 nmol mol^{-1}; ppbv) increase in global mean surface ozone abundance (Fiore et al., 2008).

However, federal and State regulations are now being developed for greenhouse gases, and methane is an attractive target for regulation due to its relatively rapid climate response and co-benefits on surface air quality (WMO and UNEP, 2011). In 2015, New York State committed to 40% reductions in its greenhouse gas emissions by 2030 relative to 1990 in its Reforming the Energy Vision (REV) goals. In May 2017, NYS announced that in order to meet these goals, it would in part specifically target in-State methane emissions as outlined in its Methane Reduction Plan (MRP).

A detailed understanding of regional methane budgets is critical for adopting successful regulatory controls, but these remain highly uncertain. Major anthropogenic sources include oil and gas production and distribution, coal mining, agriculture (livestock, manure management, and rice cultivation), landfills and wastewater treatment. Natural emissions are primarily from wetlands, but also include geologic seeps and wild animals. The global methane source is relatively well constrained due to good observational constraints on its total loss rate (550 $\pm$ 60 Tg yr^{-1}; Prather et al., 2012), but apportionment by source type and location is complicated by its long lifetime relative to atmospheric mixing timescales, limited observational constraints, co-location of major sources, and uncertainties in representing emissions (Dlugokencky et al., 2011). 1 Tg CH_4 is equivalent to 25 million metric tons of CO_2 equivalent ($MMtCO_2e$) using the 100-year global warming potential (GWP_{100}) value for methane, as has been used throughout this report.

Bottom-up emission inventories of methane have been constructed by the Environmental Protection Agency (EPA) and others, which report U.S. anthropogenic contributions of 27–29 Tg yr^{-1} with little interannual variability since 2002 (EPA, 2016). However, top-down estimates from inverse-modeling studies constrained to discrete flask samples from tall towers or aircraft and/or satellite observations

have found higher values of 30–45 Tg yr^{-1}, with the oil and gas (O&G) and livestock contributions particularly underestimated (Miller et al., 2013; Wecht et al., 2014; Turner et al., 2015) (Figure 4). A recent study reported observational evidence for a 30% increase in U.S. methane emissions from 2002 to 2014, which would account for 30–60% of the observed global changes (Turner et al., 2016).

Figure 1. Historical Methane Abundances in ppbv

Measured from Antarctic Ice-Core Bubbles
(Blue Line) and Ambient Surface Air (Gold Line) for the Past 800,000 Years

Source: Etheridge et al. (1998), Loulergue et al. (2008), and the National Oceanic and Atmospheric Administration (NOAA) Global Monitoring Division (GMD).

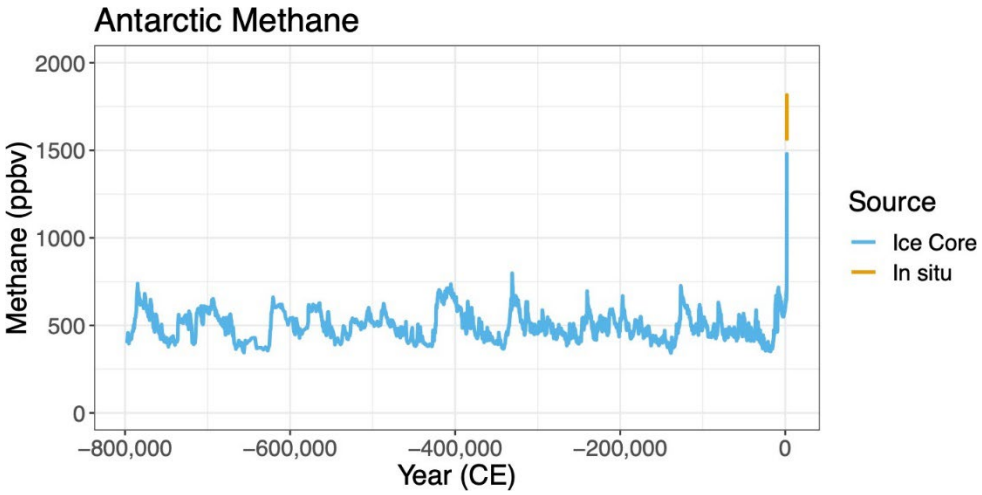

Figure 2. Methane Emissions by Source Type in MMtCO2e yr^{-1}

Left: World (18,400 MMtCO2e yr^{-1}) Right: NYS (26.5 MMtCO2e yr^{-1})

Source: Global values are from Saunois et al.(2016). New York State values are taken from this study.

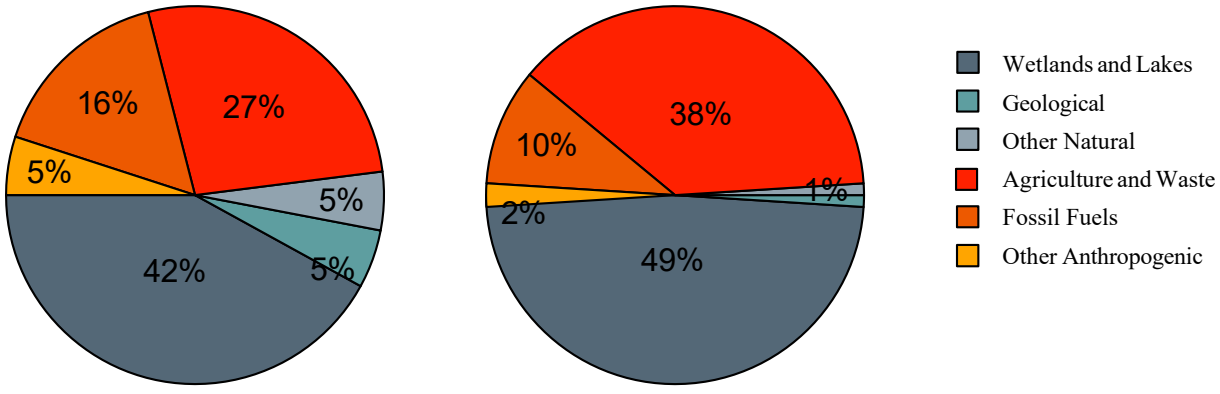

Figure 3. State-Level Gross Annual Production of Natural Gas

Source: US EIA in million cubic feet (MMcf).

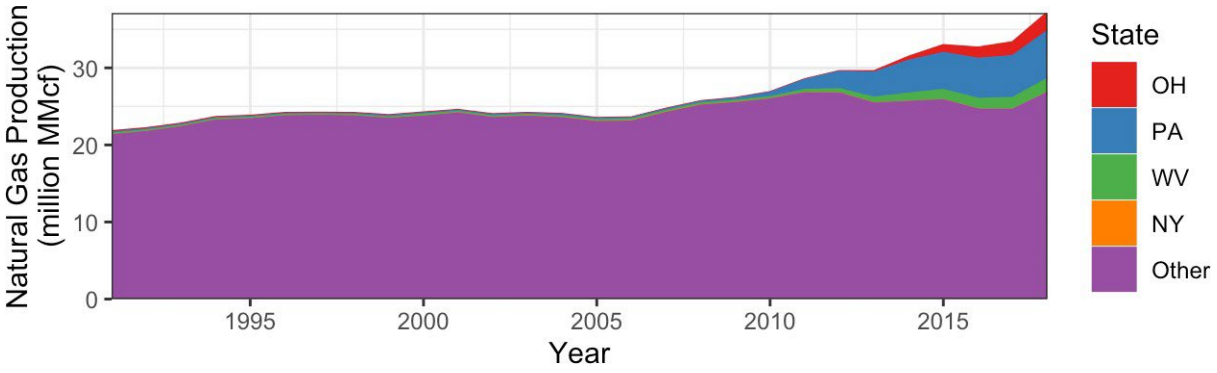

Figure 4. Large Discrepancies between Recent Estimates of U.S. Anthropogenic Methane Emissions

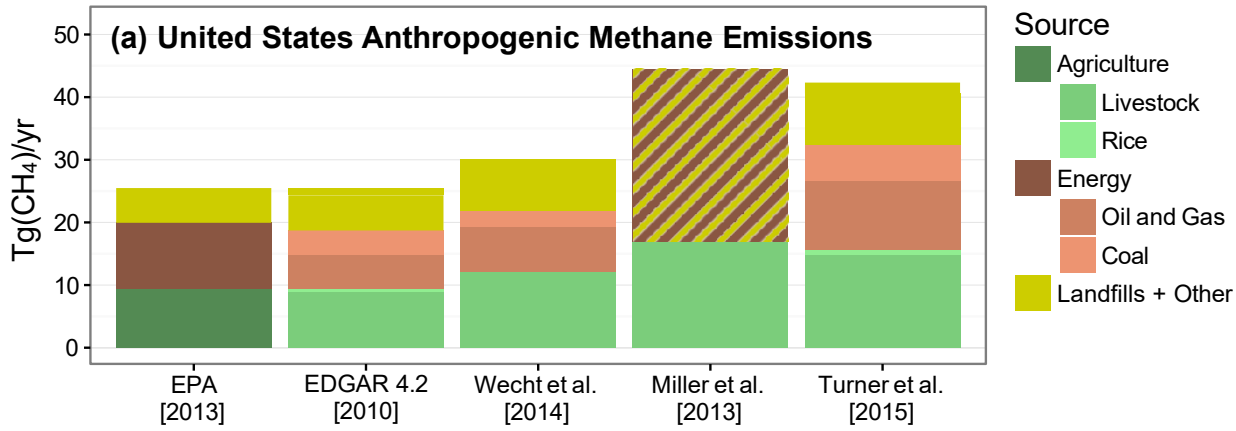

A potential candidate for such an increase is the recent surge in U.S. natural gas production and consumption, respectively +60% and +29% over the past 10 years according to the U.S. Energy Information Administration (EIA). There has been a twelve-fold increase in production in the Appalachian Basin during that period (Figure 3), primarily due to large-scale application of fracking to low-permeable shale reservoirs in Pennsylvania, Ohio, and West Virginia. NYS recently banned fracking statewide following an extensive Environmental Impact Study (EIS), which included air quality impacts; regional modeling performed by the NYS Department of Environmental Conservation (DEC) suggested that surface ozone might increase by 1-3 ppbv from in-State fracking, and called for establishment of monitoring stations (NYSDEC, 2015). Despite the local fracking ban, NYS is still a major consumer of unconventional natural gas, and susceptible to emissions from in-State conventional production, leaky distribution infrastructure, and upwind extraction activities.

The primary objectives of this project are therefore to:

1. Establish continuous methane monitors in NYS at locations well-situated to constrain major anthropogenic methane emission sources within and upwind of NYS.
2. Develop an optimized regional gridded methane emission inventory for the State by assimilating the new observations within the adjoint of the GEOS-Chem chemistry-transport model (CTM).
3. Assess the role of local versus background methane emissions on New York State and regional air quality and climate with forward sensitivity simulations.

This report summarizes our results at the end of the initial award period, with ongoing analyses to be submitted to the peer-reviewed body of scientific literature.

2 Methods

2.1 Measurements

2.1.1 Equipment Setup

Our network deployed three greenhouse-gas analyzers across NYS in order to establish extremely precise and continuous long-term measurements of methane. Although methane is the focus of this project, our instrumentation setup was also designed to measure and calibrate CO_2 to equivalent standards.

Extremely precise instrumentation is required in order to accurately capture changes in methane that can be related back to recent emissions. This is because long-lived greenhouse gases like methane and CO_2 remain in the atmosphere decades-to-centuries before removal and are therefore globally very well-mixed. Methane abundances in our measurements vary by only ± 2.9% (and ± 4% for CO_2). Furthermore, only a portion of this measured variability results from recent emission, with a large portion coming from variations in global and North American background concentrations that are transported to New York State at any given time (see section 2.2.2.1 and Figure 15). Meanwhile, it is critical that measurements used for emission estimates be regularly calibrated against equally precise reference gases in order to establish accurate absolute values, correct for any temporal drifts, and accurately compare our individual instruments to one another.

The following subsections describe our instrumentation setup, sampling and calibration strategy, and quality assurance/quality control (QA/QC) methods employed in order to guarantee the most precise and accurate measurements possible.

2.1.1.1 Picarro G2301 Cavity-Ring Down Spectrometer

The Picarro G2301 Analyzer uses cavity ring-down spectrometry (CRDS) to provide simultaneous, precise measurements of methane, CO_2, and water vapor at ambient levels for lab, field, or mobile applications (Crosson, 2008). The G2301 measures methane with precision of less than 1 ppbv with negligible long-term drift and is insensitive to changes in ambient temperature. Results are compliant with international ambient atmospheric monitoring networks, including the World Meteorological Organization (WMO) and the Integrated Carbon Observation System (ICOS). The instrument reports dry mole fractions of all measured species automatically corrected for water vapor abundance (for which there is an interference with the methane and CO_2 measurement). The analyzer can be operated in unattended monitoring stations.

Figure 5. Schematic of Picarro Analyzer Setup

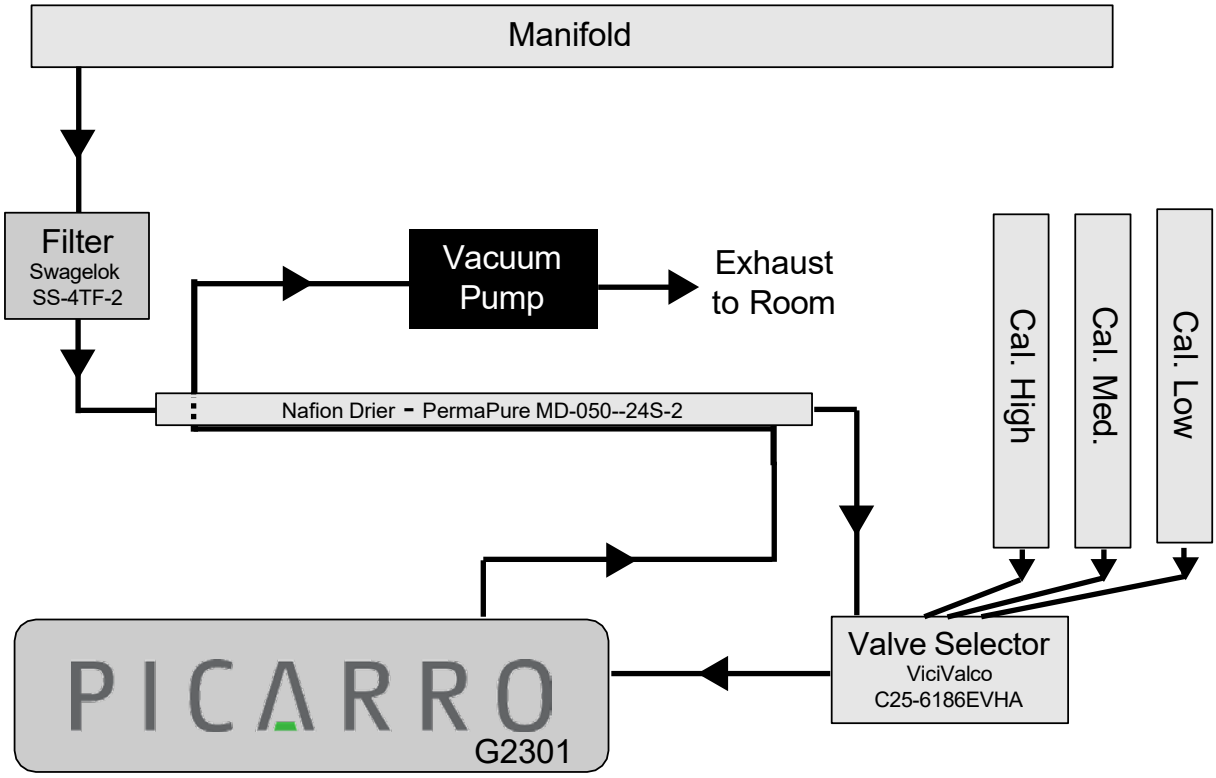

2.1.1.2 Sampling and Calibration Manifold Description

Figure 5 shows how each Picarro Analyzer is set up to sample ambient surface air and go through automated calibration sequences. The setup was designed to mimic a neighboring network in New England as described by McKain (2015).

Each Picarro Analyzer is connected to a vacuum pump that draws air into the instrument. The analyzer and pump share a common APC Uninterrupted Power Supply (UPS) battery backup that can sustain power outages of approximately 30 minutes or less; it is important that the pump and analyzer share a battery backup, as the instrument will be damaged if the pump is not running.

The inlet to the analyzer samples air from a source selected via a ViciValco rotary valve selector (model C25-6186EUHA) controlled by a serial connection to the analyzer. The valve selects between a line connected to the sampling manifold used by the NAAQS instruments and lines connecting to the various reference gas tanks via two-stage regulators. The manifold draws ambient air from the outside via an inlet at the height specified in Table 1 using a small pump and contains a condensation trap to prevent liquid water from reaching the instruments. The ambient air to the Picarro is passed through an additional submicron filter to remove particulate matter (PM) and may be additionally passed through a PermaPure Nafion drier (model MD-050-25S-2) to further help prevent liquid water from reaching the instrument cavity and to minimize any water vapor interference with the measurements; the drier requires counter-flow for dehumidification, which we provide using the analyzer purge gas.

Nine reference standard tanks were acquired from Scott-Marrin, Inc. (now Praxair, Inc.) containing methane and CO_2 ranging from low- to high-ambient concentrations. The tanks were then calibrated using a Picarro Analyzer against the same National Oceanic and Atmospheric Administration (NOAA) primary standards held by Harvard University used to calibrate the Boston network (McKain, 2015). NOAA operates as the WMO's Central Calibration Laboratory for CO_2, methane, nitrous oxide (N_2O), sulfur hexafluoride (SF_6), and carbon monoxide (CO), therefore maintaining the international reference standards for greenhouse gas measurements. The Scott-Marrin tanks were then distributed between the three sites as space allowed.

Periodically—usually every 25 hours—a program runs on the analyzer that rotates through each calibration tank for 10 minutes before returning to ambient air and records the time of each valve change. The first five minutes following valve rotation are discarded to purge the air that sat in the lines. The second five minutes are then used to compare to the known values in the reference tanks. Picarro Analyzers are robustly linear in their calibration and require only two known reference points to correct. Here, we use two-point or three-point linear corrections (pending number of available reference tanks) to adjust the instruments to match the reference standards. We interpolate the correction slope and intercept in time between calibration sequences to account for instrument drift. Over the first few years, there has been relatively negligible drift in the pre-calibrated methane measurements, and slightly greater drift in CO_2.

The analyzers may be controlled and restarted remotely. They send data to a central processing server at the University of Rochester every 15 minutes, where the calibration sequence is run hourly, and a 60-minute mean value centered on each hour is determined. Live data is streamed to the University of Rochester Atmospheric Modeling Group research website.[1]

2.1.2 Locations

The analyzers are placed at sites hosting existing NYS DEC and EPA air-quality monitoring equipment (Figure 6 and Tables 1-2). This provides contemporaneous measurements of a variety of additional chemical species that may be used in analyses, including source attribution (e.g., see section 3.2); to that end, we deployed Picarro Analyzers to three of the four most-instrumented DEC sites. However, increased speciation comes with a trade-off, as the DEC ambient air-quality monitoring sites do not sample from towers but from inlets close to the ground (Table 1). The greenhouse-gas measurement community generally prefers sampling from tall towers whenever possible (typically 30–300 meters above ground level [magl]) to increase the geographic footprint that each sample can see (e.g., see Figure 7). Furthermore, the DEC sites are generally not co-located with any NYS Mesonet weather stations (the Whiteface Mountain Base [WHT] site is a notable exception), making evaluation of the local boundary layer height more challenging.

Figure 6. NYS DEC Ambient Air-Quality Monitoring Network locations

Continuous greenhouse gas measurements have been initiated at the three circled sites, Pinnacle State Park (Addison), Rochester, and Whiteface Base.

Source: NYS DEC

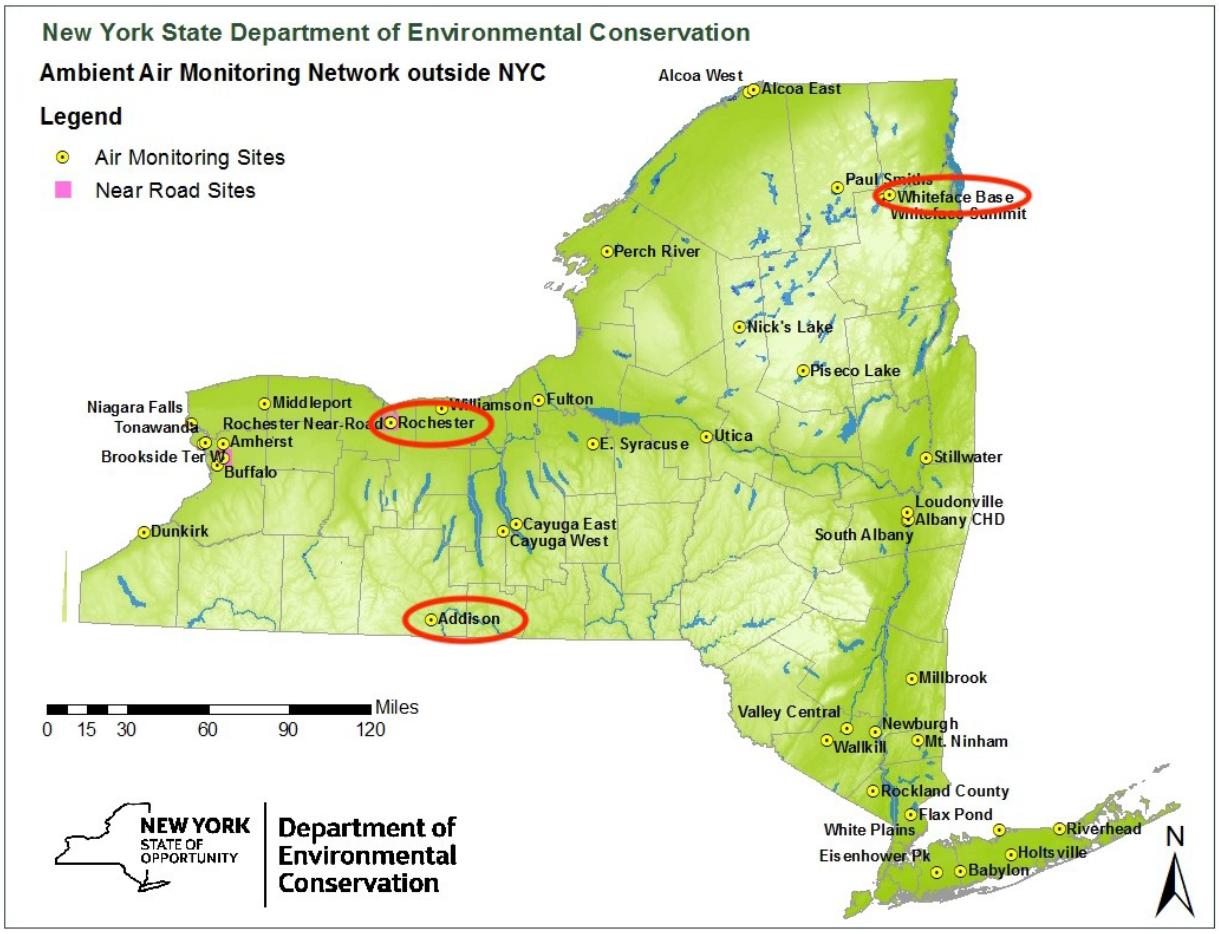

2.1.2.1 Pinnacle State Park

Pinnacle State Park (PSP) is a State-owned golf course located seven miles north of the New York/Pennsylvania border in the Southern Tier region of southwestern NY. Figure 8a shows the location of PSP on a hilltop to the southeast of the Village of Addison in Steuben County. Except for the golf course and some farmland, the surrounding area is heavily wooded with mostly mixed-deciduous hardwoods (maple, beech and birch). The closest airport is the Corning-Elmira Regional Airport (ELM), 23 miles to the east-northeast. The closest NYS Mesonet site is Addison (ADDI), 5 miles to the southwest. Prevailing winds are from the west, except in September, when they are from the south.

Table 1. Sampling Site Location Details

ID	Site	City/Town	Latitude (◦N)	Longitude (◦W)	Elevation (masl)	Inlet Height (magl)
PSP	Pinnacle State Park	Addison	42.09142	77.20978	507	4.47
ROC	Rochester	Rochester	43.14618	77.54215	137	4.74
WHT	Whiteface Mountain Base	Wilmington	44.39308	73.85890	599	4.47

Table 2. Contemporaneous Long-Term Chemical Species Sampling per Site

ID	CO_2	CH_4	C_2H_6	CO	O_3	SO_2	$NO_{\not x}$	NO_y	HNO_3	PM-ultrafine
PSP	✓	✓	✓	✓	✓	✓	✓	✓	✓	✓
ROC	✓	✓		✓	✓	✓	✓	✓		✓
WHT	✓	✓		✓	✓	✓	✓	✓		

ID	PM2.5	PM10	PM-composition	BC	Hg	Toxics	Carbonyl	PAH	NH3
PSP	✓	✓	✓	✓		✓			
ROC	✓	✓	✓	✓	✓	✓	✓	✓	
WHT	✓		✓	✓		✓	✓		✓

PSP has been selected to serve as one of the 17 EPA rural National Core (NCore) Multipollutant Network sites as well as one of their $PM_{2.5}$ Chemical Speciation Network (CSN) supplemental sites. PSP is operated by the University of Albany Atmospheric Sciences Research Center (ASRC) for NYS DEC. In addition to those listed in Table 2, PSP hosts various research projects, including temporary sampling of full-reactive nitrogen speciation and hydrogen sulfide (H_2S) during our measurement period.

Methane and CO_2 have been sampled continuously at PSP since October 2017, with ethane (C_2H_6) sampling capabilities (and a presently disabled $\delta^{13}CH_4$ sampling capability) added in November 2019.

2.1.2.2 Whiteface Mountain Base

The Whiteface Mountain Base (WHT) site is located at the ASRC Field Station of the University of Albany in the Adirondack High Peaks. Figure 9a shows the location of WHT, roughly 40% up the northeastern flank of Whiteface Mountain (summit of 1,483 meters) and about 2 miles west of the Hamlet of Wilmington in Essex County. The site is heavily forested with regional montane species (red spruce, balsam fir, birch, and sugar maple). The closest airport is the Saranac Lake/Adirondack Regional Airport (SLK), 20 miles to the west. The closest NYS Mesonet site (WFMB) is co-located with the measurement trailer. Prevailing winds are from the west-northwest although the site is prone to complicated wind conditions common to mountain monitoring sites.

Figure 7. Sensitivity of Emission Footprint to Sampling Height

Spatial footprints for July 2018 in Rochester shown for the actual sampling height (4.74 m) versus two different hypothetical tall-tower measurements (100 and 300 m). Footprints estimated with the Stochastic Time-Inverted Lagrangian Transport Model (STILT) and North American Regional Reanalysis (NARR) meteorology.

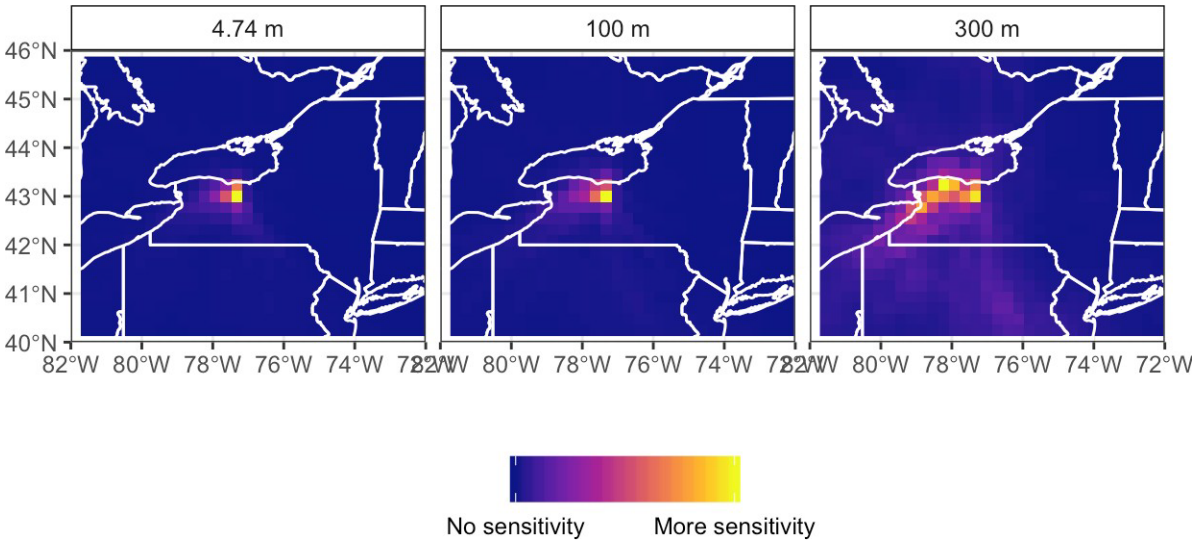

WHT has been selected to serve as one of the United States Geological Survey's (USGS) National Atmospheric Deposition Program (NADP), National Trends Network (NTN), and Ammonia Monitoring Network (AMoN) sites and; furthermore, is one of EPA's Clean Air Status and Trends Network (CASTNet) sites. Consequently, in addition to those listed in Table 2, WHT hosts a wide variety of instrumentation characterizing composition of atmospheric deposition.

Methane and CO_2 have been sampled continuously at WHT since November 2017.

2.1.2.3 Rochester

Rochester (ROC) is an urban sampling site located at a Rochester Gas & Electric (RG&E) power substation in the Rochester, NY. The urban area (MSA population of 1 million; third largest in NYS) is located in the Lake Ontario plain and Erie Canal/I-90 population corridor. It is the DEC's major monitoring site in Upstate New York. Figure 10a shows the location of ROC to the southeast of downtown Rochester. Figure 10b shows more detail of the immediate local surroundings. The site

is located immediately adjacent to CSX/Amtrak rail lines and northwest of a portion of the freeway (I-490/I-590/NY-590 highway interchange) called the "Can of Worms." The closest airport is the Rochester/Monroe County International Airport (ROC), 7 miles to the west-southwest. The closest NYS Mesonet site is Rush (RUSH), 12 miles to the south-southwest. Prevailing winds are from the west year-round.

Figure 8. Pinnacle State Park Sampling Site

(a) Aerial photograph; (b) Site surroundings; (c) Sampling manifold; (d) Instrument (Oct. 2017–Oct. 2019).

ROC has been selected to serve as one of the EPA's 63 urban NCore Multipollutant Network sites, as well as a $PM_{2.5}$ CSN and a National Air Toxics Trends Station (NATTS) site (sampling 100+ additional pollutants). It has also been selected as a site for the USGS NADP NTN and Mercury Deposition Network (MDN) programs.

Methane and CO_2 have been sampled continuously at ROC since April 2018.

In contrast to the rural sites, ROC is an urban site and therefore presented unique challenges for constraining emissions. If a site is located too close to a major point source, then its ability to constrain weaker upwind sources will be severely limited. Similarly, if the site is always located within the local urban "bubble" of elevated methane, then it would be difficult to separate local urban from regional background conditions. Ideally, we would want the site to see a mixture of air masses from both urban Rochester and background Western New York.

Figure 9. Whiteface Mountain Base Sampling Site.

(a) Aerial photograph; (b) Site surroundings; (c) Sampling manifold; (d) Instrument (Oct. 2017–Mar. 2019).

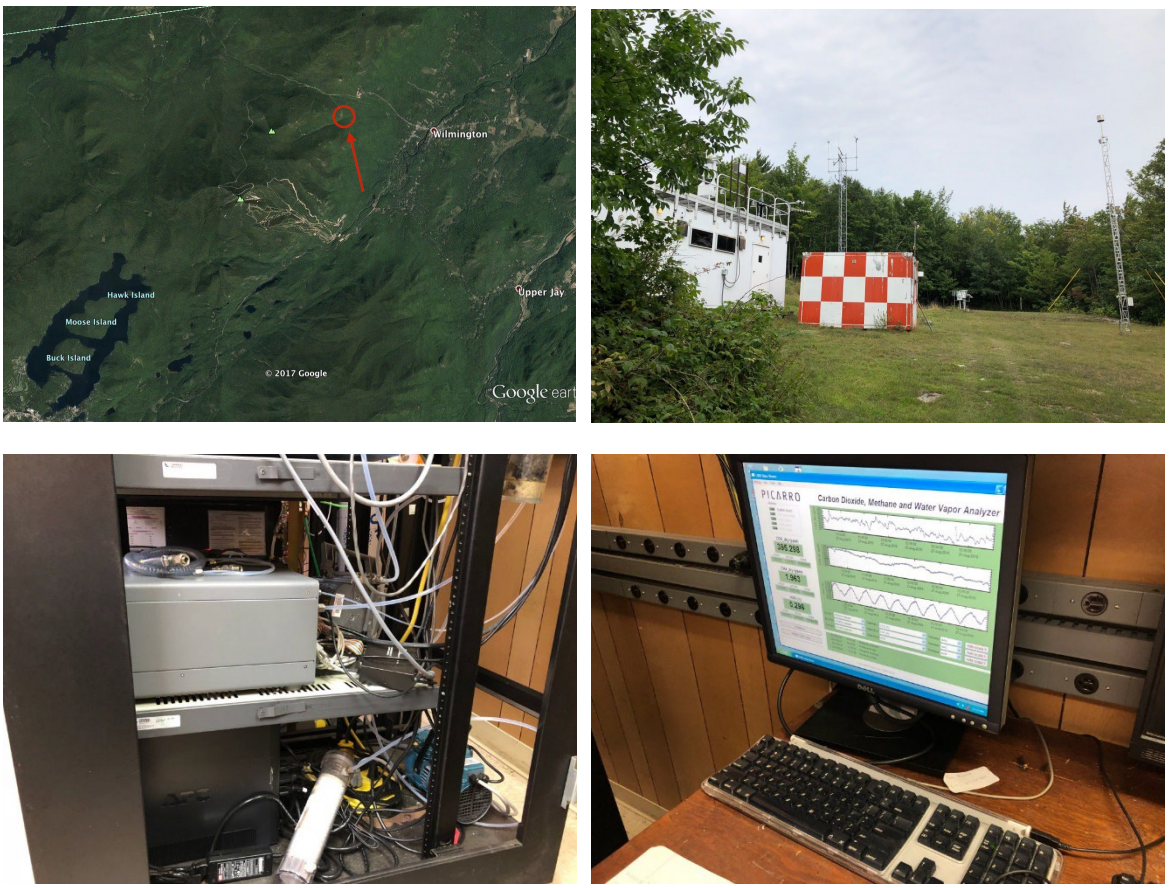

In order to evaluate the suitability of the site, we first drove the Picarro Analyzer around Monroe County before deployment to the fixed site. Our mobile sampling occurred during March when the biosphere was still inactive. Figure 11 shows the measurements taken on March 12, 2018. The highest methane concentrations in the region are located southwest of downtown, near where the interstate natural gas transmission pipelines feed into the city's local distribution network (Figure 12). The monitoring site

is on the periphery of the geographic methane maximum, and therefore, able to see local urban and regional background air masses. In addition, the Mill Street Landfill in Churchville, southwest of Rochester, was sampled as a major regional point source. There was also evidence of leaky transmission and distribution lines across the entire region that will be the target of future analysis.

Though we focus on methane, it is worth noting that the CO_2 measurements at ROC pose even more complications given the close proximity of the site to major transportation point sources (railroad and major highways). Cursory examination of the data do not show strong biases (e.g., no strong correlation to NYSDOT traffic counters on I-490 and NY-590), but we do not recommend the use of the ROC CO_2 data for emission studies at this time without further detailed evaluation.

Figure 10. Rochester Sampling Site

(a) Aerial photograph; (b) Location detail; (c) Site surroundings; (d) Sampling manifold and instrument.

2.1.3 Quality Assurance/Quality Control Protocols

The Picarro Analyzers are calibrated against standards calibrated to the international reference standards for greenhouse gases (see section 2.1.1.2 for details).

QA/QC occurs in two steps. First, when the data are initially processed, any points flagged with alarms by the analyzer are immediately rejected. These usually result from the instrument momentarily failing to maintain the strict pressure (140 Torr) and temperature (45ºC) required in the sample chamber. An hourly mean and standard deviation is initially calculated and any data points more than ± 3 standard deviations from the mean are flagged as outliers (due to instrument errors or extremely short-lived transient events), and the hourly mean and standard deviation are recalculated. Second, the central processing server at the University of Rochester generates daily summary files such as Figure 13. These are manually inspected periodically for potential errors. Usually this is due to human contamination or a leak, which manifests as a spike in CO_2 and water vapor, without an obvious shift in meteorology or methane. Faulty points are then manually flagged for removal and the day is reprocessed.

To date, all data from Oct 2017 through April 2020 have been calibrated, filtered, and evaluated for QA/QC. They are available via email request to lee.murray@rochester.edu. These data are shown and discussed in section 3.1.

Figure 11. Mobile Sampling of Methane in the Rochester Metropolitan Region

The ROC monitoring site location is indicated by the yellow star. Several observed point sources are highlighted.

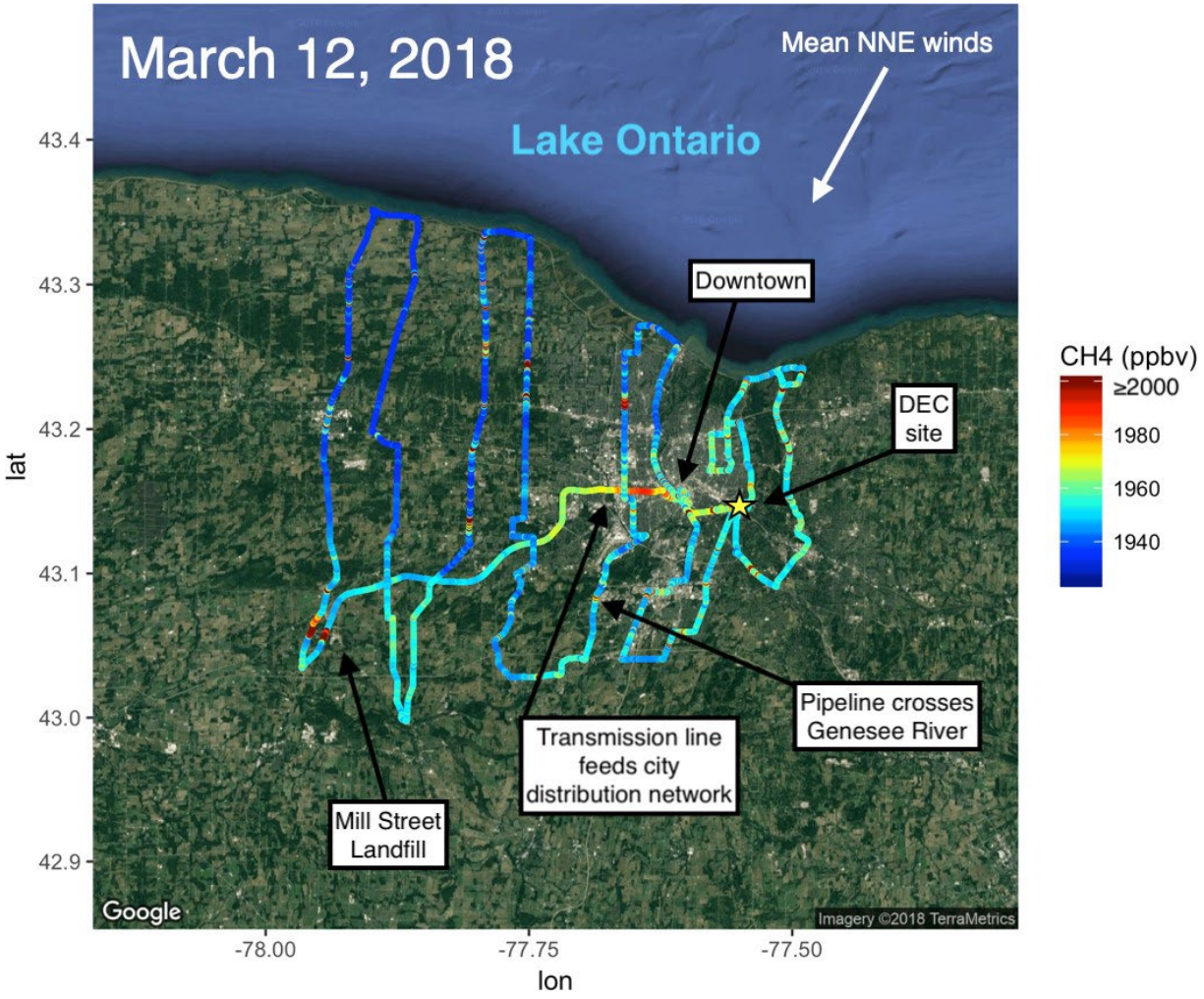

Figure 12. Inter- and Intra-State Natural Gas Transmission Pipelines (Blue) in Monroe County, NY (Yellow Border)

The transmission lines feed into the local city distribution lines at the red dot. The ROC monitoring site location is indicated by the yellow star. Source: U.S. Department of Transportation (DOT) Pipeline and Hazardous Materials Safety Administration (PHMSA), National Pipeline Mapping System (NPMS).

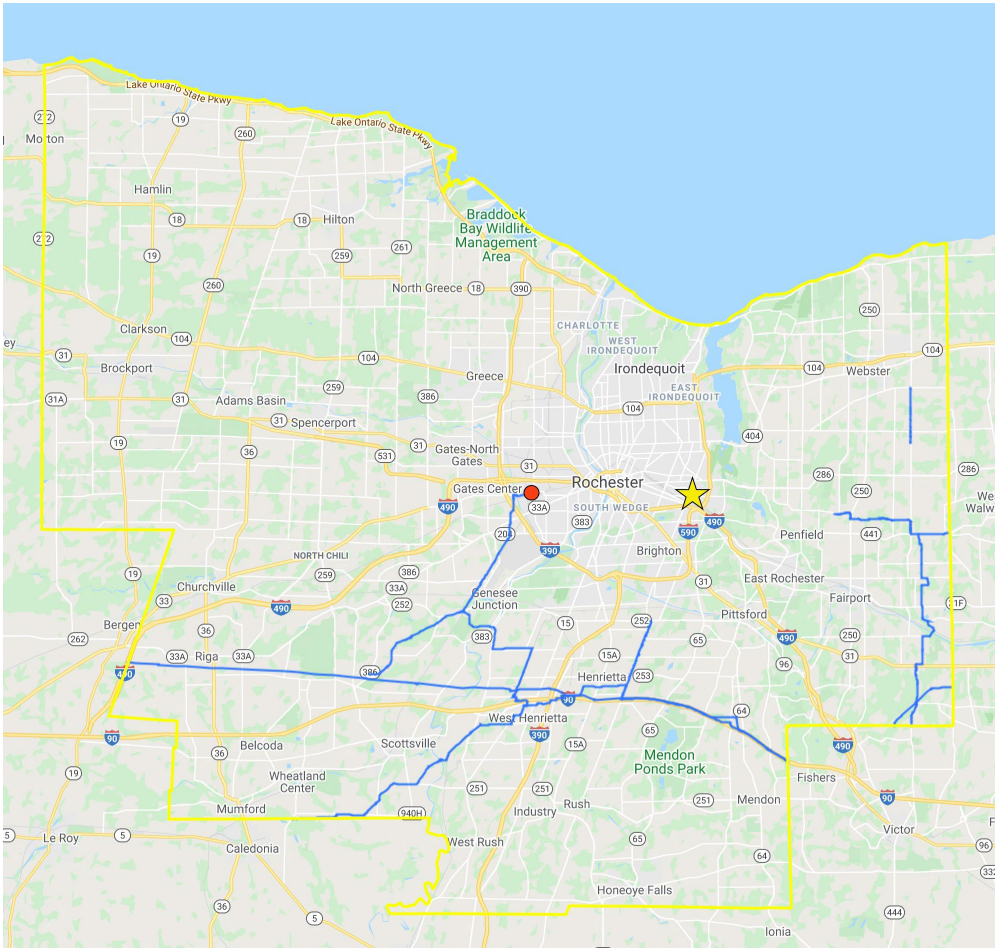

Figure 13. Example Daily Summary QA/QC Plot for May 5, 2018 at ROC

Light blue (gray) dots show raw (calibrated) data. Yellow dots and vertical error bars show the hourly mean ± one standard deviation. Blue and red dots show samples taken against the reference standards (horizontal dashed lines). Light green dots show data automatically removed. Meteorology is shown from each nearest airport and includes sea-level pressure (SLP), temperature (T), dew point temperature (Td), and wind speed and direction (black vectors). The CO_2 time series show points automatically flagged as outliers throughout the day and during purging of the lines of the calibration sequence that ran from 04:00–04:20 Coordinated Universal Time (UTC). Manual inspection indicated a likely human contamination around 20:00 UTC that was subsequently removed before the data was reprocessed.

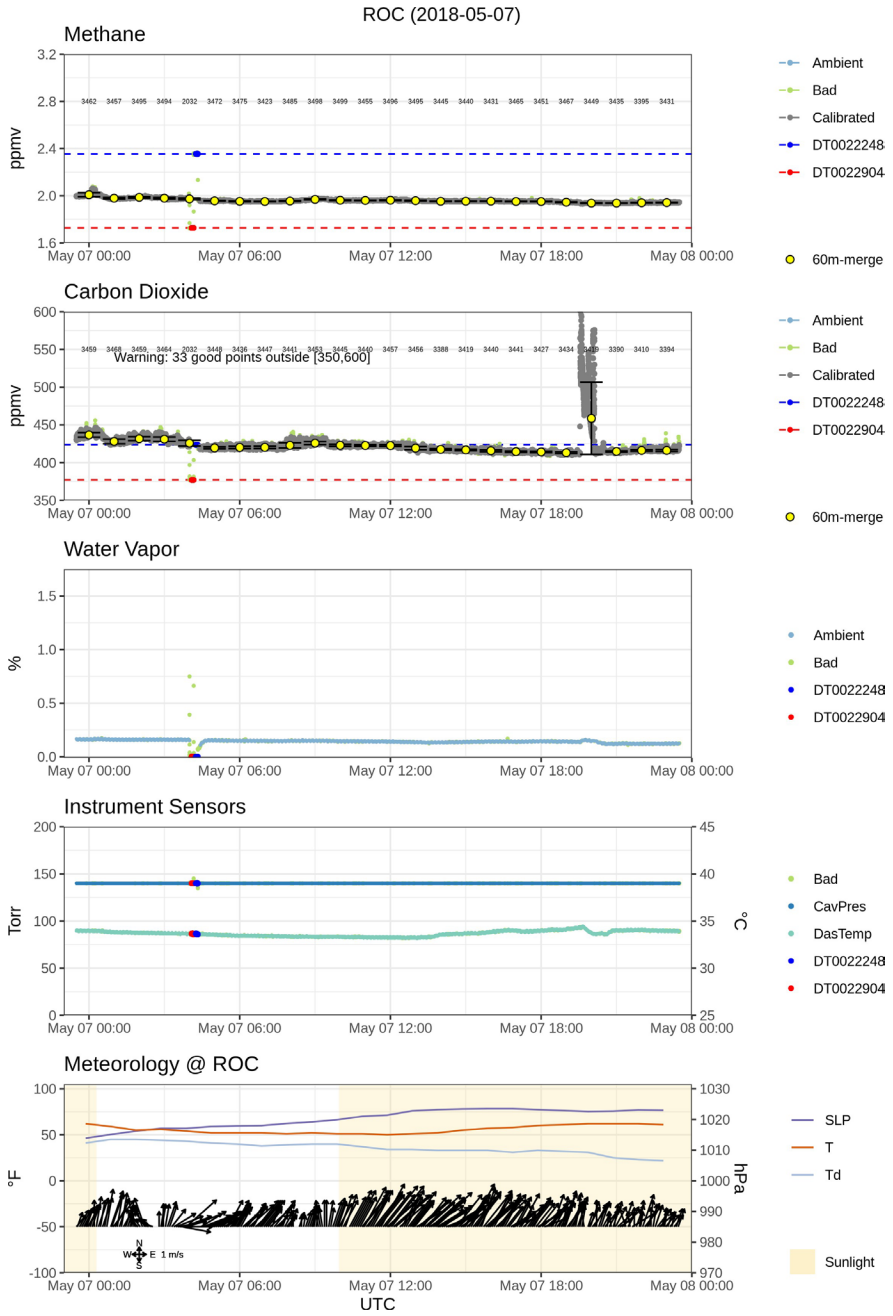

2.2 Modeling

2.2.1 Model Description

GEOS-Chem[2] is a multiscale three-dimensional (3-D) model of atmospheric composition driven by assimilated meteorological observations from the Goddard Earth Observing System (GEOS) of the National Aeronautics and Space Administration (NASA) Global Modeling and Assimilation Office (GMAO). It is developed and used by a grassroots research community worldwide as a versatile tool for application to a wide range of atmospheric composition problems from global to regional scales. GEOS-Chem is regularly updated, benchmarked, and continually evaluated by its user base. The GEOS data are available from NASA GMAO as a continuous archive from 1980 to present. The most recent GEOS-FP product has a horizontal resolution of 0.25◦ latitude × 0.3125◦ longitude (roughly 28 km × 25 km over NYS), with 72 levels in the vertical. GEOS-Chem has been frequently applied to study North American air quality (e.g., Zhang et al., 2011; Fiore et al., 2014). The model is distributed under the permissive MIT License and is readily compiled and able to be run on MacOS or Linux systems using open-source compilers.

For this project, we developed a new model capability to run for a regional Northeastern United States (NEUS) domain, as shown in the bottom panels of Figure 14. The ability to run GEOS-Chem at any arbitrary regional domain became a standard feature in version 12.4.0. The model source code may be downloaded from the GEOS-Chem public repository,[3] and all model input files (e.g., meteorology, emissions) may be downloaded from their own repository hosted by ComputeCanada.[4]

An adjoint of GEOS-Chem[5] (has been developed for performing inverse problems (Henze et al., 2007). Inverse (or “top-down”) simulations ask the opposite question of a forward (or “bottom-up”) simulation. The latter asks: “Given a set of emissions and winds, what is the downwind evolution of methane in space and time?” The former asks the converse: “Given the temporal evolution of methane at a given location and (reverse) winds, what was the upwind emission?” An “adjoint” is a computationally efficient way to explore the relative influence of many parameters (e.g., methane emissions from tens of thousands of model grid cells) within a CTM on a limited number of model outputs (e.g., hourly surface concentrations at our surface measurements).

In practice, the GEOS-Chem adjoint works as follows:

- The forward model is run using the initial emission estimate to generate synthetic measurements at the location and time of the real observations.
- The synthetic and real observations are compared to determine the model error.
- The model is then run backwards in time to propagate the model-observation mis-match backward from its measurement location to its upwind emission.
- The emissions error is then used to generate scaling factors for the original emissions.
- Steps 1-4 are repeated with the updated emissions in order to generate new emission scaling factors.
- Step 5 is repeated again and again until eventually the model converges on its optimal emission estimate, i.e., repeating Step 5 does not yield any new change.

Some recent applications of the GEOS-Chem adjoint relevant to this work include estimation of methane emissions from satellite-based observations (e.g., Wecht et al., 2014; Turner et al., 2015).

2.2.2 Simulation Descriptions

2.2.2.1 Methane Emission Optimization

Developing an optimized top-down constraint requires three sequential steps:

1. **Development of Initial Emission Estimate**
   Inverse methods like those employed by the GEOS-Chem adjoint ultimately determine their optimal solution as a weighted average of (a) the initial emission estimate and (b) that predicted by the model and observations, with the relative contribution of each determined by the relative uncertainties in each (cf. Ch. 11 of Brasseur and Jacob (2017)). The more accurate the initial emission estimate, the more accurate the optimized solution, so it is important to work from the most accurate initial estimate available. Our baseline anthropogenic emissions inventory is the bottom-up Emissions Database for Global Atmospheric Research (EDGAR) v4.3.2 (Crippa et al., 2018), with methane emissions available by individual sector for fossil fuels, livestock, landfills, waste management, rice cultivation, and other various anthropogenic sources. The data is available as gridded annual means for the period 1979–2012 at 0.1◦ × 0.1◦ horizontal resolution. Seasonal scaling factors for manure use and rice cultivation are applied following Maasakkers et al. (2019). Biomass burning emissions (mostly agricultural waste burning in the tropics) are prescribed from the daily near-real time emissions of the NASA Quick Fire Emissions Database (QFED) to provide realistic changes in a source that is highly variable in space and time. Over the United States, instead of EDGAR, we use the Gridded Environmental Protection Agency (GEPA) inventory of Maasakkers et al. (2016) for fossil fuel, livestock, landfill, waste management, and rice cultivation. This inventory is consistent with the na- tional EPA Greenhouse Gas Inventory (EPA, 2016), but with spatial and monthly variability derived from bottom-up methods. The GEPA inventory is available at 0.1◦ × 0.1◦ hori- zontal resolution per sector for the continental US. For Canada and Mexico, we use the EDGAR base inventory for all anthropogenic sources except the O&G sector, for which we apply the inventory of Sheng et al. (2017).

Figure 14. Initial Emission Estimates Separated by Natural (Left Column) and Anthropogenic Sources (Right Column) for April 2018-March 2019

Units are log-transformed metric tons of CO_2 equivalent per sq km per year. See text for description.

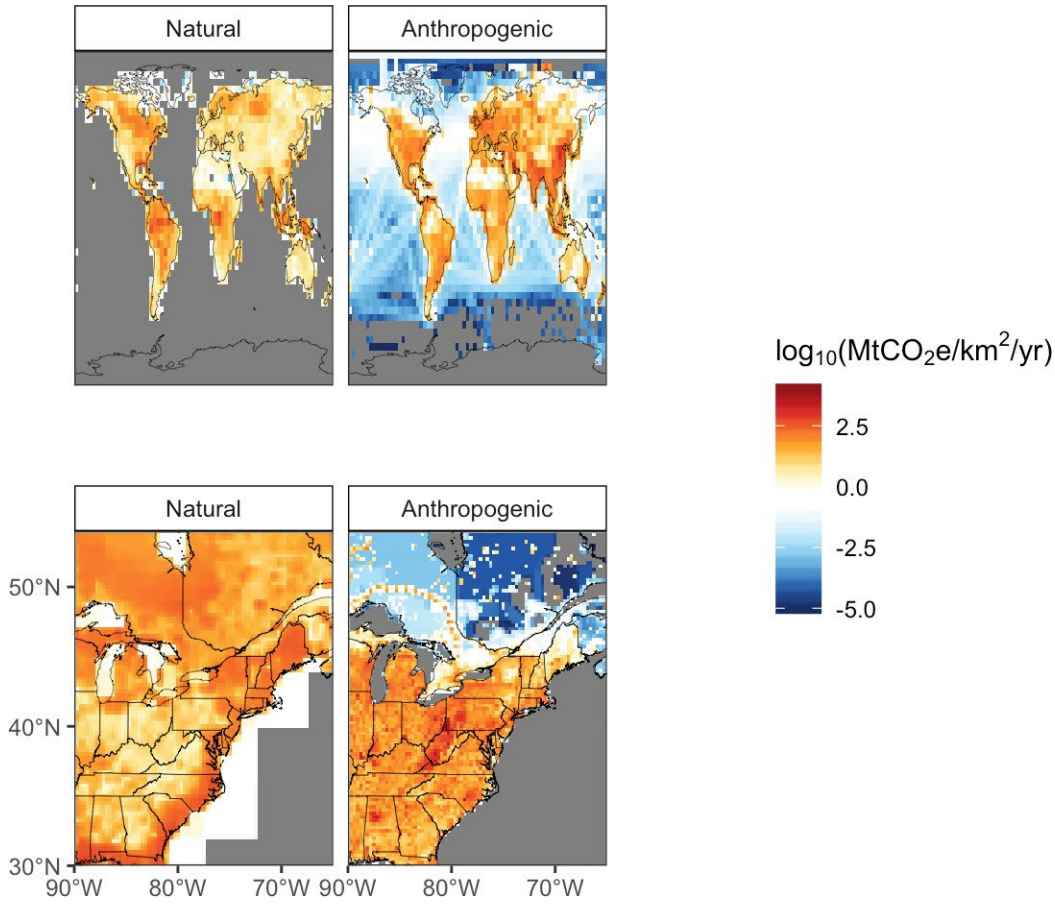

Figure 15. Example Simulated Background and Total Methane Time Series at PSP for October 27 to December 31, 2017

The background is estimated by running the model with no emissions (red line) versus a simulation including NEUS emissions (black line). The difference between the two is the contribution due to recent upwind NEUS emission. Variability in the background can at times be up to half of the total variability.

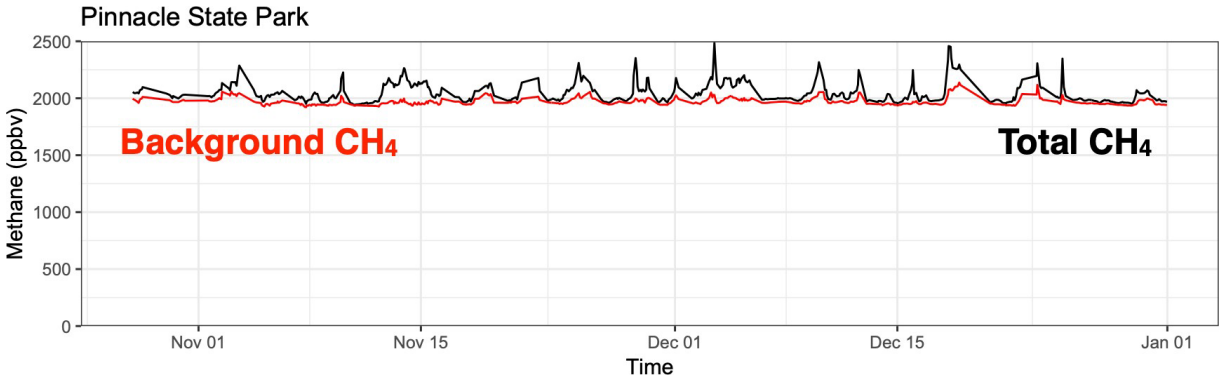

Natural processes are primarily wetland emissions from version 1.0 of the "WetCHARTs" inventory (Bloom et al., 2017), scaled to match the total emissions from Kirschke et al. (2013). The data is available as monthly means for the period 2009–2015 at 0.5◦ × 0.5◦ horizontal resolution. Natural emissions also include the termite source and soil absorption (applied as negative emission) from Fung et al. (1991) and the geological seeps inventory from Maasakkers et al. (2019). Where inventories do not exist for our exact analysis period, we use the most recently available year of data.

Figure 14 shows the natural and anthropogenic initial emission estimates we use for our global (top row) and regional (bottom row) domains. In NYS in the initial estimate, anthropogenic emissions dominate in Western New York, the Hudson Valley, New York City and Long Island, are comparable to natural emissions throughout most of Central New York and are dominated by natural emissions in the Adirondacks and Catskills.

2. Generation of Regional Boundary Conditions

In order to achieve fine spatiotemporal resolution over NYS, computational requirements dictate that we limit the spatial domain of our simulation to the Northeastern United States (NEUS), as shown in the bottom row of Figure 14. This requires that we prescribe the temporal evolution of methane at the boundaries of our domain for our regional simulation. This is especially important for methane since variations in the so-called "background" (reflecting shifting winds and upwind emissions) can be an important component of variability measured at a given site. For example, Figure 15 demonstrates the magnitude of background variability at the PSP site. If one assumed that the background concentration was constant, background variability would instead be erroneously attributed to local recent emissions.

Therefore, we first must perform a global simulation using the GEOS-Chem adjoint in order to determine optimized boundary conditions by assimilating available methane observations from outside the NEUS domain. Of particular utility due to its information density is the new methane column product from the European Space Agency (ESA) TROPOspheric Monitoring Instrument (TROPOMI) satellite (Hu et al., 2018). The TROPOMI methane product is available at approximately 7×3.5 km^2 horizontal resolution and daily near-global land coverage beginning in April 2018. Therefore, we selected our analysis period to be May 2018 to April 2019 in order to use the TROPOMI data to constrain our boundary conditions. However, the first-generation TROPOMI product has known data quality issues when ground pixels contain variable surface reflectivities (such as along coastlines or croplands), manifesting as non-physically low or high values. Therefore, we removed the bottom and top 20th percentile of data at a given surface elevation (columns are naturally thicker at lower elevations) from our analysis to avoid these outliers.

The GEOS-Chem adjoint was run for 99 iterations from May 2018 through May 2019 at global 4◦ latitude × 5◦ longitude horizontal resolution. We used the residual method in order to estimate the observational uncertainty (Heald et al., 2004), assumed 100% uncertainty in our initial boundary conditions, and assumed that model errors correlated with a 25 km length scale (see Ch. 11 of Brasseur and Jacob [2017] for more detail on these assumptions). TROPOMI total methane columns were assimilated in order to optimize the time-varying concentration of methane at the surface and at 500 hPa for every three-hour period between May 1, 2018 and June 1, 2019.

3. Assimilation of Observations to Optimize Emissions

Once we have an initial emissions estimate and optimized boundary conditions, we may then assimilate all available methane observations in our domain of interest to optimize local emissions.

Figure 16 summarizes the location of data assimilated in our inversion. In addition to PSP, WHT and ROC, we also obtained hourly methane time series data from sister networks upwind and downwind of NYS. These include 3 sites in New England provided by Harvard University (McKain, 2015), 6 sites in Ontario and Québec provided by Environment and Climate Change Canada (ECCC) (Pugliese et al., 2018), and 11 sites in the Mid-Atlantic provided by the U.S. National Institute of Standards and Technology (NIST) (Karion et al., 2020). The NIST data included two additional sites in NYS that complement our network in geographic coverage (Utica in the Mohawk Valley and Mineola on Long Island). Furthermore, we obtained tower and aircraft data from the end of the NASA Atmospheric Carbon & Transport-America (ACT-AMERICA) suborbital field campaign,[6] which was available through May 2018. We also aggregated TROPOMI methane columns within our NEUS domain.

The GEOS-Chem adjoint was then integrated again for 99 iterations from May 2018 through May 2019 at its native 0.25◦ latitude × 0.3125◦ longitude horizontal resolution. Once again, we used the residual method in order to estimate observational uncertainty (Heald et al., 2004), assumed 100% uncertainty in our initial emission estimate, and assumed that model errors correlated with a 25 km length scale. The surface, aircraft and satellite observations were assimilated in order to optimize gridded methane emissions over the period May 1, 2018 through April 30, 2019.

Figure 16. Observations Used to Constrain New York Methane Emissions

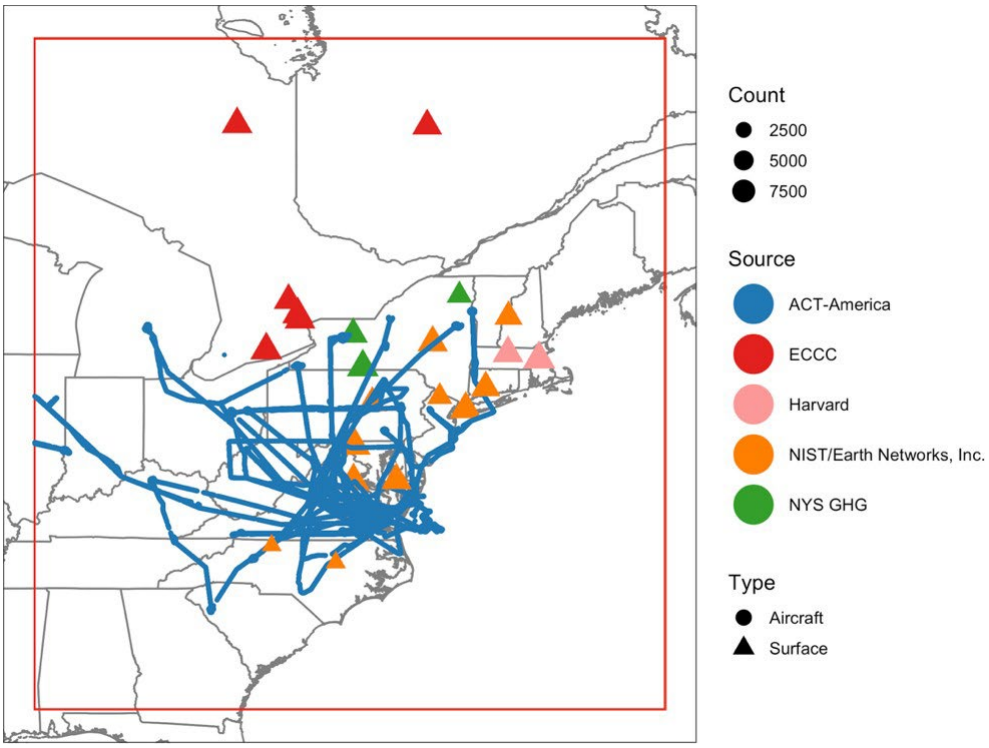

2.2.2.2 Impact of Upwind Oil and Gas Activities

In addition, we performed photochemical simulations exploring the impact of upwind O&G emissions from the Marcellus region for the 2017 summer ozone season (June-August). First, a global photochemical simulation using the standard GEOS-Chem emission inventories for version 12.6.0 was performed in order to generate boundary conditions for our NEUS domain. Then the boundary conditions and emissions (namely, the EPA National Emissions Inventory version 2011 (NEI2011) and Canadian Air Pollutant Emission Inventory (APEI) emission inventories) were used to integrate over the smaller spatial domain for our period of analysis. We then performed a sensitivity test in which we prescribe and remove the Marcellus-region O&G VOC emissions using our optimized emissions and examined the impact on downwind air quality.

3 Results

3.1 Measurements

Figure 17 shows the hourly mean abundances of methane (top row) and CO_2 (bottom row) measured at Pinnacle State Park (PSP) (left column), Rochester (ROC) (middle column) and Whiteface Mountain Base (WHT) (right column).

Greenhouse gas abundances are highest at the urban site (ROC) and lowest in the Adirondacks (WHT), with both gases an average 3.6% higher in Rochester than at Whiteface. Both methane and CO_2 abundances grew in surface air across NYS during our measurement period. Methane grew at a rate of 13–24 ppbv yr^{-1}, faster than the global background average rate of 10 ppbv yr^{-1} calculated by NOAA.[7] Similarly, CO_2 grew at a rate of 3–7 parts per million by volume (≡ 1 μmol mol^{-1}) (ppmv) yr^{-1}, faster than the global average rate of 2.5 ppmv yr^{-1}. The faster growth rates reflect higher emissions over land than the ocean, and do not necessarily reflect local emission trends. However, variations between sites within New York State will partially reflect spatial differences in local emissions.

For methane, hour-to-hour changes have a greater magnitude than the seasonal cycle or long-term trends in abundance. Methane abundances peak in winter when demand for space heating peaks and methane's photochemical-loss rate is at a minimum.

Figure 18 is the same as Figure 17, but the data is limited to the afternoon when the boundary layer is thoroughly mixed. Some of the variability is reduced in the methane time series, but otherwise, the trends and patterns remain consistent.

3.2 Source Attribution

Next, we take advantage of contemporaneously measured species to characterize the air masses at each site. Of particular interest is the covariance of methane and CO_2 with carbon monoxide (CO), which is available from NYS DEC at PSP and ROC. All three have common sources from fossil fuel consumption, are chemically linked (methane oxidizes to CO which oxidizes to CO_2), and entrainment of background air into plumes will dilute their trace gases by common ratios. However, fresh methane emission (e.g., due to O&G extraction or leaky transmission) is uncorrelated with either CO or CO_2. Meanwhile,

methane and CO_2 both have opposite nocturnal biospheric cycles, while CO has no biospheric component. Therefore, we may apply a simple principal component analysis (PCA) (e.g., Thurston and Spengler , 1985) to these three gases to characterize the relative air masses sampled at each site.

Figure 17. Hourly Mean Greenhouse Gas Abundances Measured in Surface Air of New York State since October 2017

Mean abundances and growth rates are given for the 24-month period of May 2018 through April 2020 for each site and gas (black line and text). Monthly mean value shown as yellow dots.

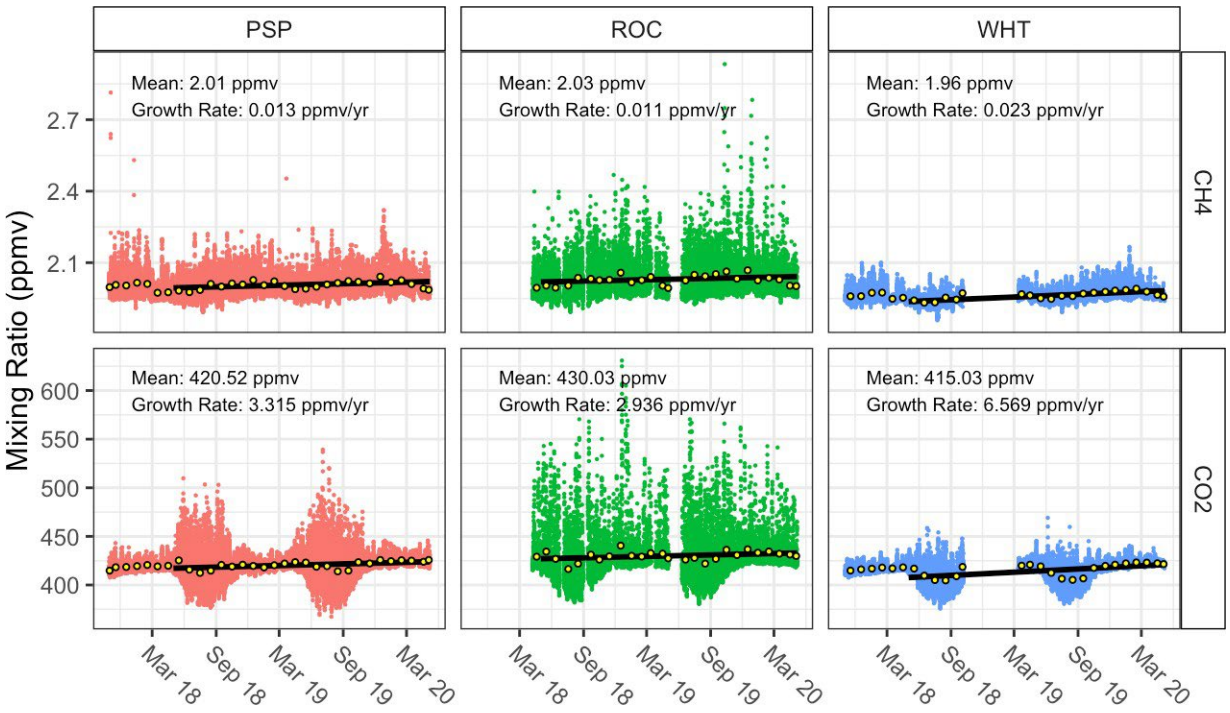

Table 3 summarizes the results of the PCA for PSP and ROC. PCA takes the time series of each of the three gases and transforms the data in a way that pulls out major patterns of covariance. Fifty-four percent of the time at PSP, the three gases are correlated with each other, characteristic of aged air masses that have been transported to the site. Thirty-one percent of the time methane and CO_2 are strongly anti-correlated (mostly reflecting nighttime respiration of the biosphere). And 15% of the time, methane is strongly anti-correlated with CO and CO_2, indicative of recent methane emission. The ROC time series tells a similar story, although its second mode of variability is less likely controlled by the biosphere, and more likely controlled by CO emitted from the adjacent railway and Interstate highway. We can conclude that both PSP and ROC see air masses indicative of recent fresh methane emission at least 10% of the time.

3.3 Sensitivity of Observations to Local Emission

Figure 19 estimates where our network is able to constrain upwind emissions with statistical confidence. Formally, this is the ratio of remaining uncertainty to initial uncertainty after we perform a Bayesian analytical inversion, which we calculated using a separate transport model (Stochastic Time-Inverted Lagrangian Transport Model [STILT]), since adjoint methods cannot explicitly calculate the equation. Methane emitted from anywhere that is red (values close to 0) has sufficient downwind observations that we can determine its emission flux with very high certainty. Methane emitted from anywhere that is white (close to 1) is not sufficiently sampled by any downwind sensors, and therefore its uncertainty remains high. Our three sites provide broad coverage of Western New York and the Adirondacks. The two NIST sites in New York State provide good coverage in the Mohawk Valley and downstate. In the State, our results are most uncertain in the Catskills, the Cattaraugus Mountains, and the southern Adirondacks.

Figure 18. Same as Previous Plot, but Data Limited to 11:00 AM to 4:00 PM Local Time

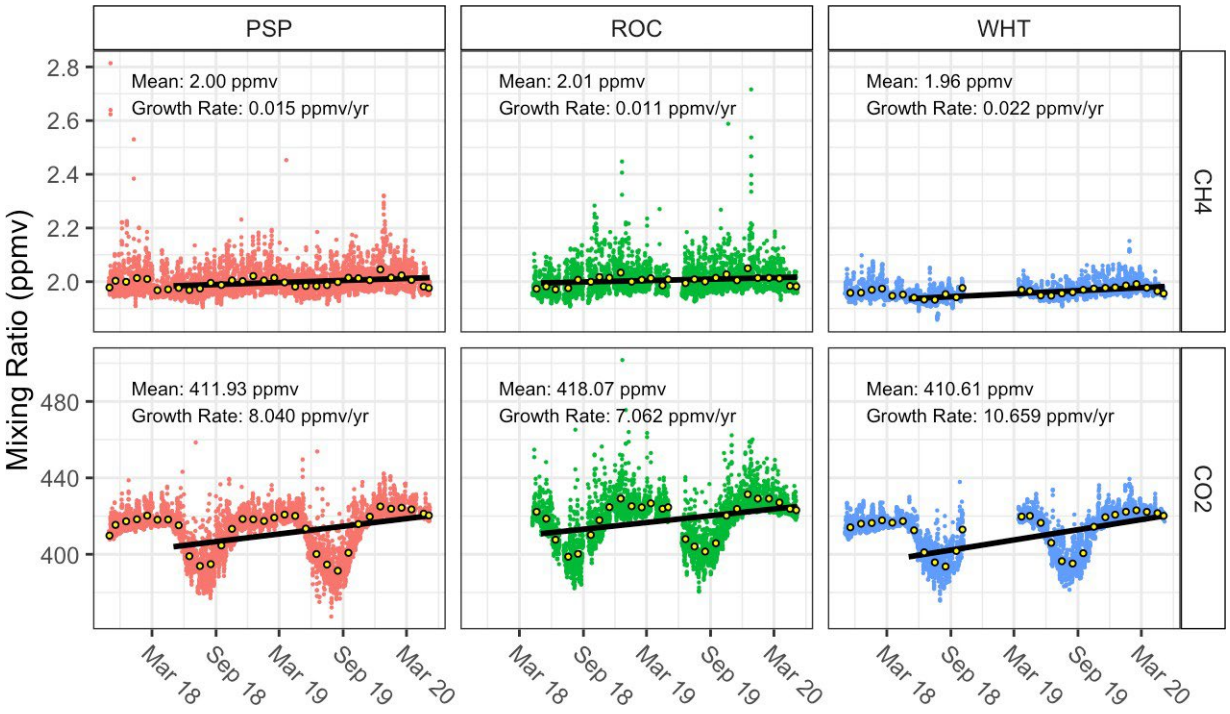

Table 3. PCA Source Characterization

Correlation coefficients greater in absolute magnitude than 0.45 are highlighted in bold.

PSP (Oct. 2017–Apr. 2020)

	1	2	3
CH_4	**0.69**	0.02	**0.73**
CO	**0.55**	**0.64**	**-0.54**
CO_2	**0.47**	**-0.77**	-.042
Variance (%)	54	31	15

ROC (Apr. 2018–Apr. 2020)

	1	2	3
CH_4	**0.62**	0.41	**0.67**
CO	**0.46**	**-0.88**	0.12
CO_2	**0.64**	0.23	**-0.73**
Variance (%)	62	26	12

Figure 19. Relative Uncertainty in Local Emissions Remaining after Emission Optimization

1 = 100 % uncertainty remains; 0 = No uncertainty remains. Calculated using the STILT model with NARR meteorology.

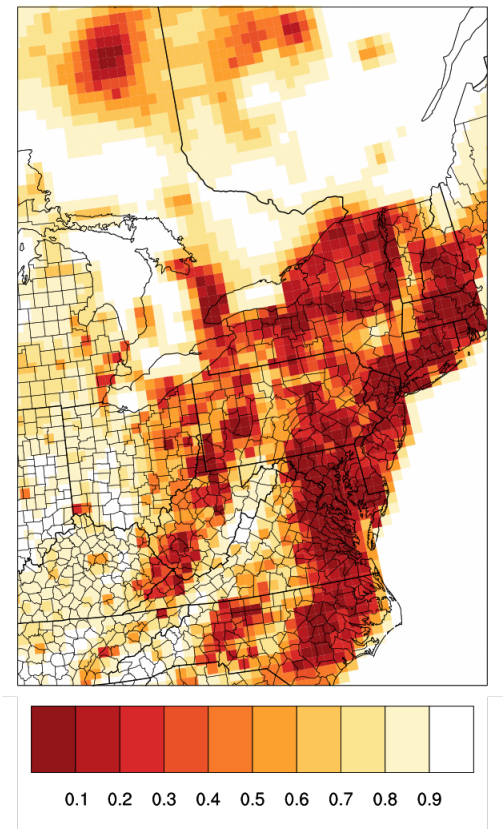

Figure 20. Hourly Mean Methane Observations for May 2018

Shown in black for Pinnacle State Park, Rochester, and Whiteface Mountain Base.

The simulated methane time series before emission optimization is shown in red. The simulated methane time series following emission optimization is shown in blue.

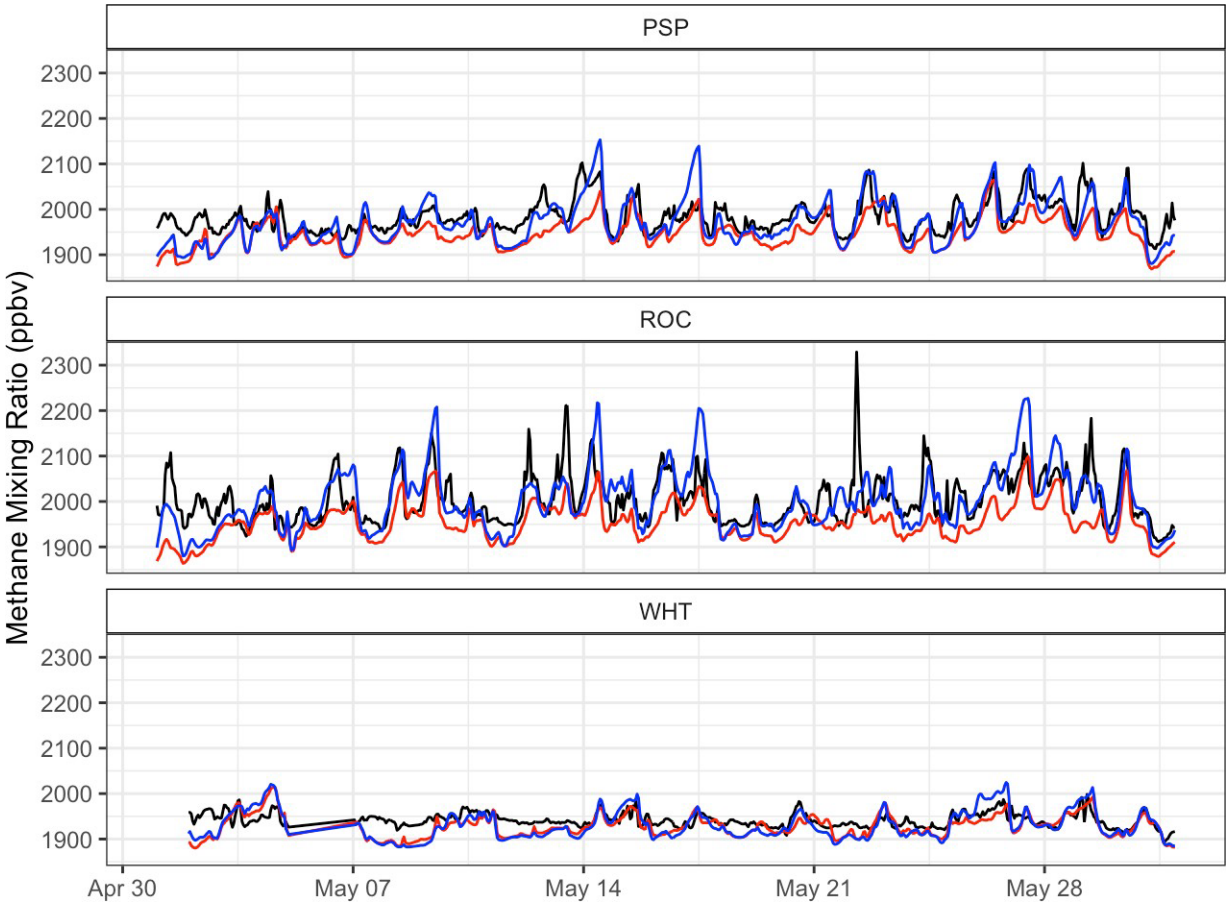

3.4 Emission Optimization

Figure 20 demonstrates the improvement in the adjoint model's ability to capture the observations (black line) before (red line) and after optimization (blue line) for a subset of the analysis window. As the model is imperfect by definition, the optimized time series does not perfectly match the observations; the optimization favors the prior emission estimate when trusting the model would be highly uncertain. Nevertheless, the optimized emissions yield the expected improvement. The absolute low bias of the model against the ensemble of in situ observations has decreased from

26 to 10 ppbv, with model-observation correlation coefficient increasing from $R = 0.61$ to 0.73 ($n = 318, 976$ over 26 sites). The TROPOMI columns also show improvement under the optimized emissions but are more modest (low bias decreases from 12.8 to 12.7 ppbv; R increases from 0.50 to 0.51; $n = 113, 067$).

Figure 21 shows the prior (left panel) and optimized (right panel) total methane emissions following the optimization. In general, the optimization found anthropogenic sources to be underestimated and the wetland source to be overestimated. In particular, large portions of Michigan, Indiana, Ohio, and Pennsylvania were increased in the optimization, although not in the regions most associated with O&G activities. The EDGAR inventory underestimates Canadian emissions, particularly in the Toronto metropolitan area. In NYS, urban areas and landfills in the Erie Canal/I-90 Corridor were underestimated, as was the area around Ithaca, New York City, and Long Island. Meanwhile, much of eastern New York State was found to be overestimated.

Figure 21. Original (Left Panel) and Optimized (Right Panel) Total Methane Emissions for May 2018–April 2019

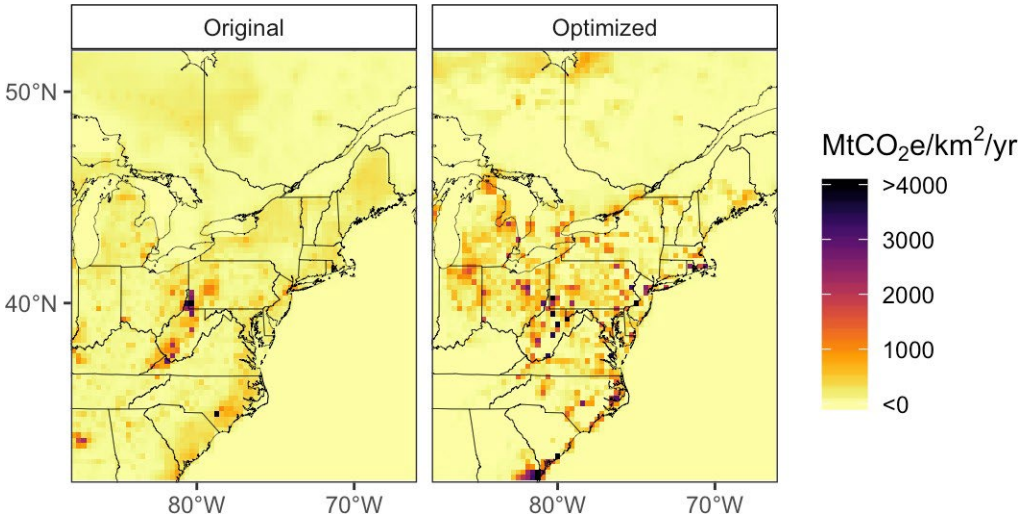

Figure 22 aggregates the optimized annual gridded flux estimates over the spatial footprint of each of the 62 counties in NYS. The constrained total emissions are then distributed across eight broad emission categories based on the relative source apportionment in the original emissions inventory (see section 3.4.1). Figure 23 shows the same figure but with a fixed color scale to help identify the counties and sectors with the greatest contributions to the statewide total. Figures 24-25 show the difference in the optimized emission estimates relative to the original emission estimates. Table 4 summarizes the numerical values for each county.

Total methane emissions are highest in Western New York, the Finger Lakes, the North Country, and Long Island. Western New York and the Finger Lakes reflect a mixture of livestock, landfills, O&G and wetland emissions. North Country emissions are primarily from wetlands. Long Island emissions are primarily due to Landfills and O&G use. It is also worth noting that while the five Boroughs of New York City have smaller aggregate emissions than many other counties, they have the highest emissions per unit area.

The greatest changes in the emission inventory occurred over Chautauqua County (attributed to wetlands, although this is quite possibly misattributed O&G emission; see section 3.4.1), Wyoming County (the greatest number of cows in NYS), and Suffolk County (attributed to landfills and O&G). Meanwhile, emissions generally decreased in the North Country due to an overestimate of the wetland source.

Figure 22. Annual Top-Down Methane Emissions Aggregated at the County Level
Units are $MMtCO_2e$

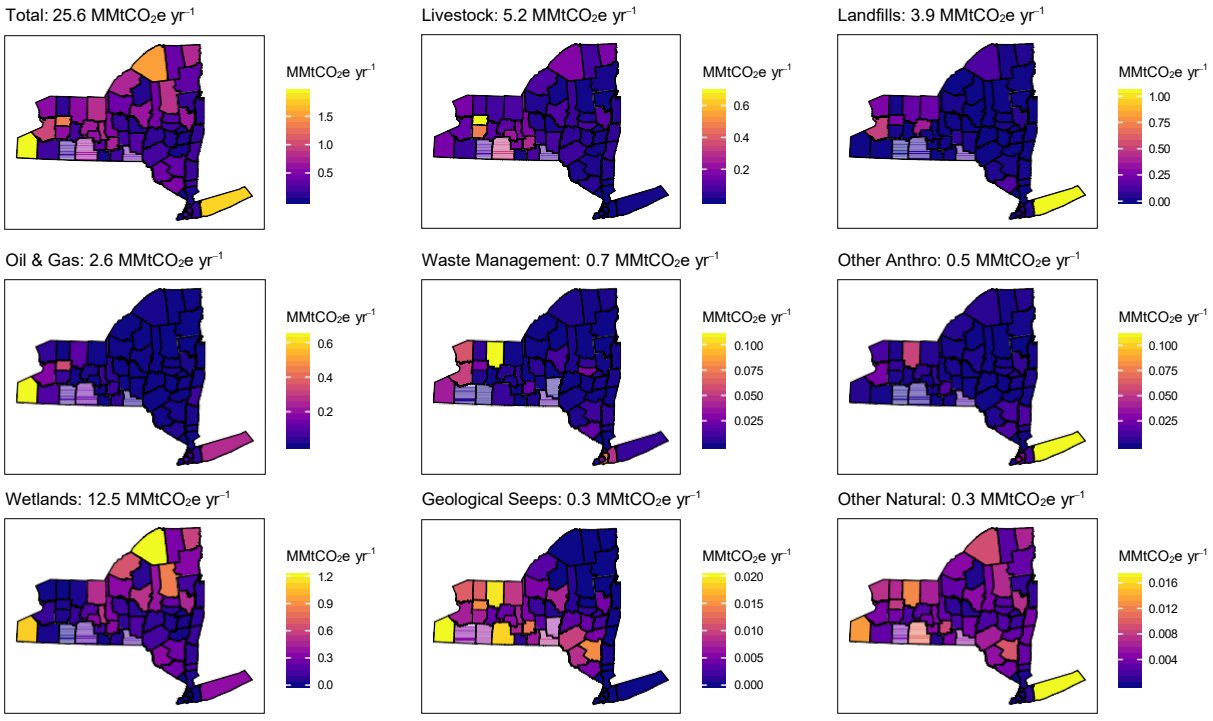

3.4.1 Discussion of Limitations

It is important to acknowledge some limitations of top-down methods as they pertain to our results.

First, the optimization is built upon probabilistic distributions; there is nothing to prevent the optimized net surface flux to be negative (i.e., a net sink) if that improves the downwind model-observation comparison. There is a globally small uptake of methane by soil microbial activity that may cause the net local flux to be negative. In fact, we do see small negative fluxes in many places in our results (particular in regions far from our observations like rural Canada and the Gulf States). However, it is probably more likely to interpret these negative fluxes as values that are statistically zero within the local uncertainty of the estimate.

Figure 23. The same Figure as Figure 22, but with a Common Color Scale for All Panels

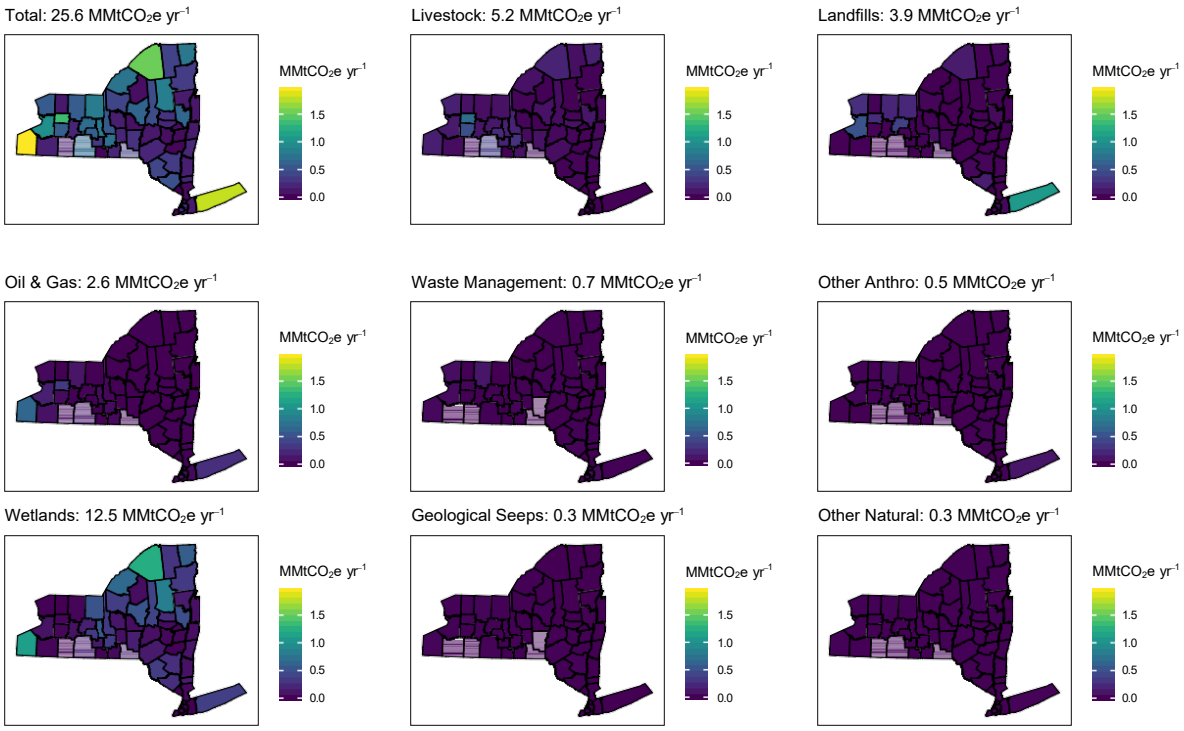

Figure 24. Change in Annual Top-Down Methane Emissions Aggregated at the County Level Relative to the Original Emission Estimate

Units are $\Delta MMtCO_2e$

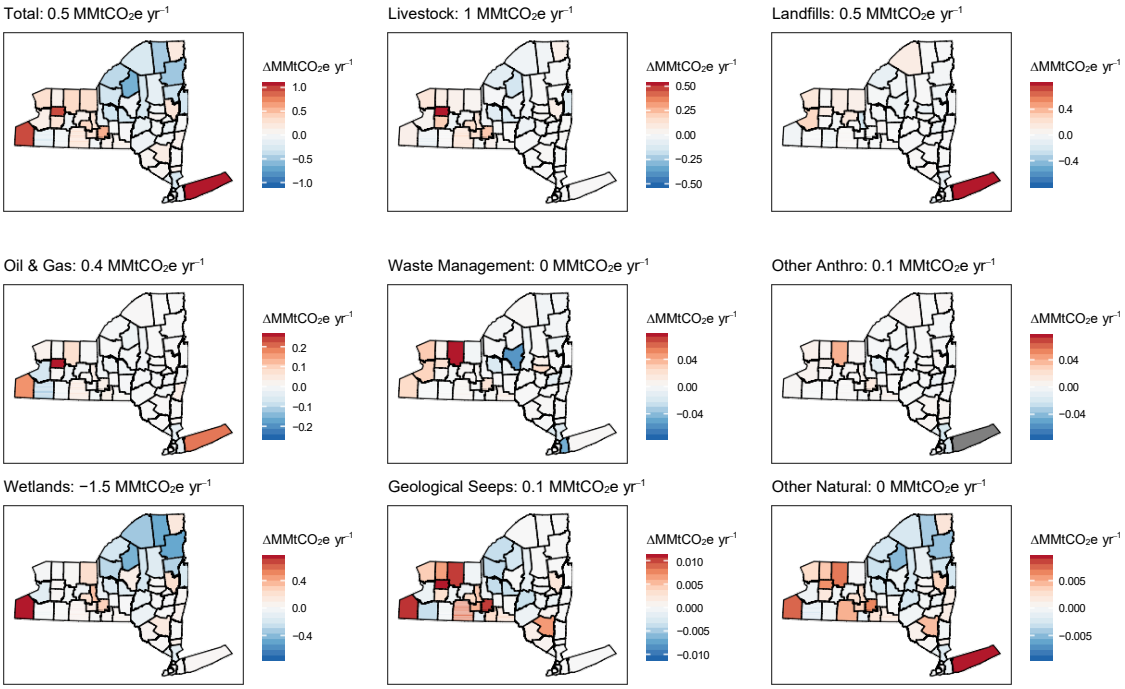

Figure 25. The Same Figure as Figure 24, but with a Common Color Scale for All Panels

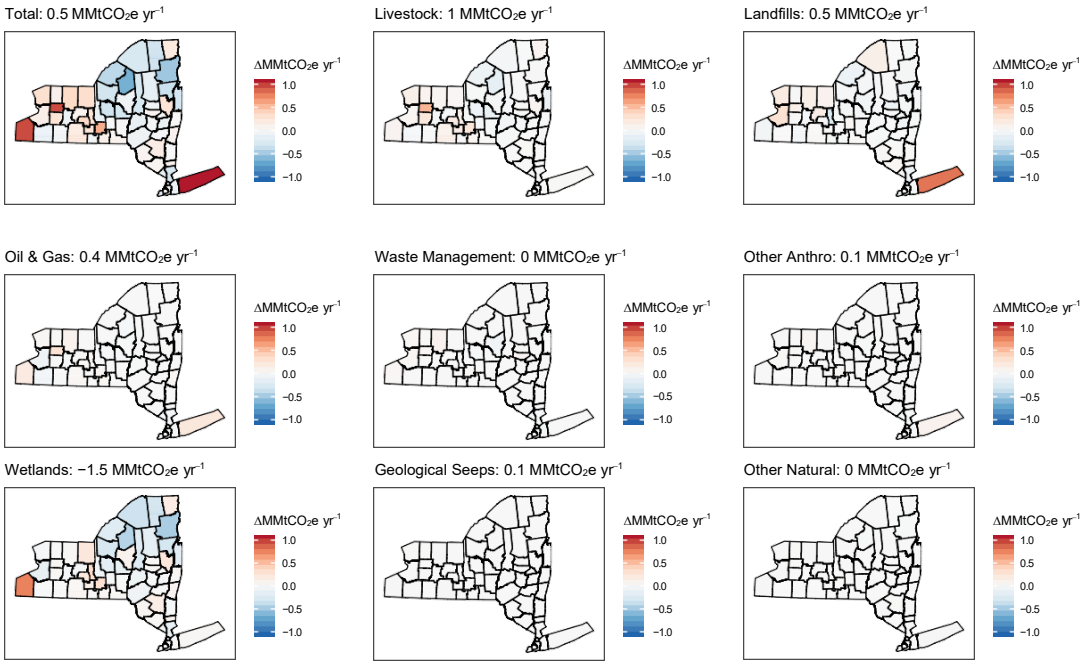

Table 4. Annual Top-Down Methane Emissions

Aggregated at the county level by sector (black text) and changed from the prior emissions estimate (red and blue text indicate increase and decrease, respectively). All units are in metric tons of CO_2 equivalent ($MtCO_2e$).

	Total		Livestock		Landfills		Oil & Gas		Waste Management		Other Anthro		Wetlands		Geological Seeps		Other Natural	
	Total	Change	Total	Change	Total	Change	Total	Change	Total	Change	Total	Change	Total	Change	Total	Change	Total	Change
Statewide	**25,617,951**	**548,538**	**5,191,041**	**995,517**	**3,937,202**	**459,647**	**2,645,327**	**391,839**	**733,083**	**45,287**	**507,417**	**84,964**	**12,541,343**	**(1,482,498)**	**283,292**	**54,235**	**254,652**	**21,832**
Chautauqua	1,934,334	924,518	161,492	46,497	2,550	(44,661)	638,857	160,534	38,024	23,219	4,309	1,322	1,080,576	733,745	20,028	10,249	13,052	7,248
Suffolk	1,771,466	1,058,043	6,383	3,718	1,041,209	781,759	257,290	186,833	7,819	1,181	109,423	74,832	356,765	14,157	0	0	17,083	9,183
St Lawrence	1,508,288	(283,501)	178,442	(36,441)	136,826	102,384	9,454	1,761	3,015	1,011	4,916	1,770	1,204,118	(361,964)	0	0	8,964	(2,511)
Genesee	1,339,929	924,932	686,038	515,601	254,084	103,497	328,992	255,416	26,136	19,644	7,590	5,628	29,491	19,463	14,521	10,861	7,856	5,876
Erie	967,822	110,948	130,551	27,456	495,746	268,304	168,927	(73,945)	51,993	26,741	25,086	3,980	91,878	(141,125)	7,233	(1,052)	4,076	(668)
Hamilton	824,401	(161,019)	3,967	(1,495)	4,179	(3,302)	254	19	81	13	147	(16)	820,227	(157,871)	0	0	6,852	(1,174)
Wayne	806,415	299,663	83,781	20,763	210,400	75,077	5,219	455	723	(3,051)	4,798	1,594	495,535	205,409	9,048	(628)	6,252	(87)
Seneca	790,754	231,884	176,795	103,999	2,288	(231,933)	57,960	26,429	5,608	1,849	6,504	4,254	536,604	324,277	7,240	4,361	4,542	2,736
Clinton	768,682	168,422	166,396	49,814	38,123	(9,194)	3,839	341	2,492	(1,782)	4,211	1,580	574,115	133,759	0	0	6,450	1,918
Jefferson	738,728	(424,369)	88,885	(92,927)	0	(104,442)	873	(3,954)	389	(2,163)	3,961	(659)	654,766	(216,836)	3,059	(3,980)	4,757	(2,732)
Tompkins	716,104	544,068	275,528	210,901	6,617	3,124	50,489	23,751	20,085	16,780	14,205	11,539	339,871	271,092	13,496	9,975	8,468	6,259
Ontario	676,738	64,263	113,933	(14,641)	365,067	127,436	15,796	(12,163)	5,031	1,336	6,516	1,760	167,708	(38,946)	3,977	(797)	2,466	(484)
Steuben	650,503	290,191	328,211	159,983	39,365	19,348	118,461	43,570	8,478	3,531	3,638	1,082	141,088	57,863	18,218	8,052	10,754	4,667
Saratoga	638,954	237,235	106,795	53,775	46,326	(26,432)	13,280	3,738	1,129	(975)	7,059	1,552	463,415	205,031	4,432	2,162	7,042	3,268
Oneida	625,992	(73,314)	88,187	(26,707)	347	(59,675)	5,218	(6,698)	11,450	(56,637)	2,758	(4,955)	512,963	80,966	7,496	28	4,908	(738)
Yates	587,933	347,481	233,150	140,583	11,716	7,189	6,705	3,759	3,004	1,788	1,256	751	327,988	191,091	5,964	3,361	3,742	2,109
Wyoming	581,896	234,446	467,870	198,298	16,565	7,973	54,365	7,482	3,617	2,146	3,307	1,757	32,403	15,221	7,202	3,000	3,896	1,623
Monroe	563,443	344,901	69,178	42,979	197,200	102,598	101,170	69,772	108,593	74,600	53,626	37,638	24,291	12,724	19,201	9,963	12,203	6,652
Niagara	550,386	287,350	164,255	104,348	260,433	149,717	38,926	17,925	59,630	29,332	12,963	6,343	8,988	(22,049)	11,612	4,184	7,285	2,780
Cayuga	533,151	(118,276)	177,370	(28,766)	3,077	(9,096)	28,624	(12,996)	855	(1,290)	1,535	(2,055)	318,259	(63,436)	5,017	(1,003)	3,208	(741)
Orange	480,617	47,513	28,891	956	142,595	27,403	19,586	1,848	18,719	200	13,489	2,481	254,474	14,162	4,862	594	4,041	266
Herkimer	445,425	(301,639)	56,914	(30,093)	568	(36,438)	2,182	(13,084)	2,386	(4,556)	625	(1,113)	384,864	(215,975)	932	(1,314)	4,135	(2,396)
Sullivan	403,056	51,670	13,033	(2,908)	32,629	11,720	4,874	479	2,946	791	3,112	726	340,721	40,050	8,320	1,177	5,220	738
Oswego	396,584	(330,660)	22,410	(8,587)	23,774	(20,178)	3,343	(1,131)	647	(707)	1,700	(1,268)	341,274	(296,139)	4,986	(4,218)	3,131	(3,173)
Franklin	380,109	(500,346)	72,415	(28,649)	18,401	116	1,469	(586)	1,238	(3,703)	1,338	(500)	293,482	(480,859)	0	0	2,591	(4,354)
Broome	346,743	128,942	61,099	21,162	87,588	22,527	20,056	10,523	15,029	10,263	12,436	6,781	144,664	55,341	8,511	3,399	5,340	2,133
Ulster	338,612	136,965	17,643	6,045	22,088	5,054	10,939	2,145	9,493	812	12,229	2,937	256,357	115,536	14,527	6,510	9,434	4,195

Essex	337,993	(527,873)	11,692	(10,806)	6,948	(29,069)	640	(1,080)	304	(2,382)	1,470	(1,310)	326,786	(491,173)	0	0	3,226	(4,866)
Schuyler	327,027	243,071	180,161	132,573	3,853	1,544	4,515	1,972	998	400	1,844	1,259	130,332	101,627	7,718	5,358	4,842	3,362
Fulton	277,154	(59,595)	23,113	5,849	5,323	(83,773)	3,343	910	7,451	5,476	1,759	408	237,408	11,862	57	(234)	2,627	190
Chenango	272,090	(10,405)	80,495	(5,539)	22,376	6,419	3,668	(3,597)	3,248	474	1,074	76	156,791	(8,233)	6,433	(7)	4,036	(4)
Queens	240,262	(36,118)	147	(27)	58,090	(10,119)	78,317	(15,608)	71,933	(2,295)	32,131	(6,063)	0	(2,051)	0	0	721	(94)
Kings	229,725	6,715	152	6	52,620	429	105,677	4,848	28,045	528	37,944	2,579	5,478	(1,693)	0	0	388	(36)
Columbia	208,653	70,015	46,865	6,785	3,469	(7,285)	58,829	26,999	697	(1,597)	1,494	(751)	99,242	46,382	10	(1)	3,950	1,046
Livingston	205,641	(96,372)	107,013	(31,946)	2,369	(20,056)	6,866	(21,411)	899	(1,813)	2,172	(499)	84,280	(20,288)	3,901	(682)	2,110	(371)
Montgomery	202,137	46,513	87,363	8,344	17,721	3,916	12,333	350	28,266	21,541	3,575	1,864	52,668	11,242	1,305	(546)	2,216	401
Delaware	201,472	(89,032)	59,625	(7,902)	2,928	(9,622)	1,742	(1,207)	1,449	234	891	(345)	128,206	(69,548)	9,612	(932)	6,030	(584)
Cortland	196,953	(8,478)	54,877	(15,528)	63,391	23,634	1,896	(562)	970	201	719	(170)	72,841	(15,835)	3,276	(317)	2,055	(199)
Tioga	196,712	86,092	85,428	40,310	14,669	(5,087)	41,857	25,392	2,108	1,287	2,578	1,319	45,357	20,722	6,834	3,115	4,288	1,954
Putnam	189,800	69,072	1,551	592	16,675	7,365	16,976	6,286	2,412	(1,548)	4,928	1,760	148,137	54,950	0	0	1,782	672
Cattaraugus	173,365	(222,177)	56,120	(59,948)	2,832	(13,855)	86,268	(111,442)	4,246	(1,936)	1,448	(1,449)	19,505	(31,486)	5,632	(3,939)	3,047	(2,131)
New York	170,677	52,830	109	33	1,772	571	62,649	19,095	75,527	23,670	26,962	8,279	3,774	1,217	0	0	234	71
Dutchess	158,340	(2,845)	23,212	(3,821)	17,936	4,118	12,529	(585)	6,507	(54)	14,389	3,144	84,937	(5,600)	469	(240)	3,315	(387)
Onondaga	155,575	(355,528)	24,719	(105,636)	8,391	(26,137)	5,107	(18,752)	5,441	(18,202)	2,480	(12,781)	108,268	(171,192)	1,695	(4,100)	1,064	(2,572)
Allegany	150,238	(86,482)	77,371	8,105	58	(75,821)	59,829	(20,575)	680	(587)	1,011	(283)	7,843	3,066	6,587	(739)	3,564	(400)
Bronx	145,132	(120,830)	58	(37)	96,045	(94,175)	24,123	(11,022)	15,692	(11,292)	9,291	(4,353)	0	0	0	0	154	(100)
Warren	140,049	(373,969)	801	(3,665)	5,288	(45,178)	82	(2,629)	24	(6,082)	41	(2,272)	134,425	(315,600)	0	(5)	1,238	(2,957)
Nassau	135,123	(116,326)	128	(435)	38,608	(17,969)	38,397	(35,367)	46,076	(47,056)	12,462	(15,943)	0	0	0	0	1,110	(897)
Rensselaer	127,774	706	41,426	1,878	6,542	(9,208)	6,021	(3,509)	2,453	(3,713)	2,983	(2,055)	70,212	17,822	123	3	4,017	1,033
Orleans	120,872	87,300	86,621	63,476	13,283	9,588	5,057	3,706	7,315	5,409	3,040	2,226	0	0	11,595	6,199	6,853	3,749
Otsego	118,590	(143,671)	37,059	(45,681)	1,811	(3,177)	1,450	(5,565)	393	(453)	1,020	(1,083)	74,457	(85,077)	3,479	(3,822)	2,183	(2,399)
Washington	115,928	(327,637)	31,236	(107,626)	2,043	(22,317)	772	(2,285)	1,445	(949)	1,303	(1,972)	79,634	(193,849)	37	18	1,097	(2,714)
Madison	74,883	(318,848)	11,506	(121,072)	0	(30,399)	1,062	(16,197)	3	(5,576)	293	(2,197)	61,373	(140,742)	938	(3,862)	588	(2,423)
Schoharie	73,000	(30,991)	27,363	(14,272)	0	0	2,151	(6,049)	844	(648)	433	(270)	39,548	(9,323)	3,858	(626)	2,420	(398)
Lewis	67,167	(660,029)	6,952	(159,186)	0	(29,659)	1,110	(21,098)	0	(986)	84	(597)	60,150	(449,022)	0	(3,271)	481	(5,219)
Schenectady	62,574	(5,930)	16,085	6,888	8,303	(22,169)	7,695	1,508	4,922	1,754	5,034	1,223	19,546	4,822	1,608	200	1,256	316
Albany	50,074	(119,919)	15,001	(5,070)	2,961	(68,720)	5,657	(12,213)	1,840	(12,297)	2,527	(6,487)	20,504	(14,438)	2,368	(1,097)	1,586	(814)
Westchester	47,694	(290,796)	263	(819)	0	(99,330)	6,470	(36,371)	73	(15,441)	1,180	(19,632)	39,932	(120,106)	0	0	454	(1,826)
Greene	29,299	(17,416)	8,455	(1,748)	1,133	(1,631)	1,771	(10,467)	508	(365)	894	(1,520)	13,348	(2,247)	4,720	622	3,094	121
Richmond	27,317	(168,727)	18	(111)	3	(124,407)	9,052	(11,123)	1,596	(4,367)	4,674	(4,843)	12,049	(24,027)	0	0	152	(306)
Chemung	21,538	(45,393)	8,443	(13,341)	0	(8,653)	4,264	(7,045)	103	(1,440)	551	(2,540)	7,382	(11,170)	1,153	(1,745)	723	(1,095)
Rockland	56	(118,697)	1	(771)	1	(9,994)	2	(15,691)	4	(14,982)	2	(9,501)	46	(68,195)	0	0	1	(887)

Second, top-down methods are capable of constraining the total net flux at a given grid cell but are incapable of distinguishing between co-located sources within that grid cell (e.g., a cow in a wetland surrounding a landfill). We use our prior bottom-up estimate of the partitioning of individual sources to estimate the optimized sector-level emissions, but this will simply convolve any errors that existed in the prior source attribution. For example, the WetCHARTs wetland inventory seems to be universally too high in the mid and high latitudes. Therefore, the portion that this analysis attributes to wetlands in all counties co-located with other major sources (e.g., Chautauqua's O&G or Seneca's landfills) is probably overestimated. Thus, we encourage focus on the total emission estimates when focusing on where to mitigate emissions, and then the sector-based emission estimates as a first guess of what sectors might be most effective for emission mitigation.

Lastly, adjoint methods are computationally efficient means for determining optimized estimates, but they do not provide estimates for the error bars on the optimized emissions at each location. The panel on the right of Figure 21 gives a misleading perspective on the amount of information that one can extract from the observations; in reality, confidence in the optimized emission estimates decreases with distance from the measurement locations. New York State is well characterized by our design (see Figure 19), but one should be careful when interpreting the emission fluxes in regions not well-characterized by our observations.

3.4.2 Comparison with NYS Greenhouse Gas Inventory (GHGI)

Table 5 compares our top-down total (natural + anthropogenic) emissions for 2018–19 with the bottom-up anthropogenic emissions for 2016 developed by NYSERDA and NYSDEC for the NYS Greenhouse Gas Inventory (GHGI) (NYSERDA, 2019; NYSERDA and NYSDEC, 2019). In general, the bottom-up and top-down approaches agree relatively well. The main difference between the two is a much larger landfill source in the NYS Greenhouse Gas Inventory (GHGI). However, it is quite possible that our inventory is overestimating the fraction of methane due to wetlands in Wayne and Seneca counties in the Finger Lakes (see section 3.4.1 and Figure 23), some of the largest and fastest-growing landfills in NYS presently exist. We are presently testing the use of the NYS GHGI as our prior emission estimate over New York State.

3.5 Impact on New York State Air Quality

Given its long lifetime, methane emitted within and immediately upwind of NYS has negligible impact on NYS air quality. However, upwind O&G activities are associated with the emission of shorter-lived and more reactive non-methane volatile organic compounds (NMVOC) as well as reactive nitrogen oxides (NO_x) that could have sufficient reactivity to impact downwind air quality. The fugitive NMVOCs are emitted within known ratios to methane measured from well pads. Therefore, we can use the optimized methane emissions to estimate the NMVOC emissions as well.

Table 5. Comparison of Mission Estimates with the 2016 New York State Greenhouse Gas Inventory (GHGI)

	NYS GHGI	This Work
Livestock	4.51	5.19
Landfills	10.61	3.94
Oil & Gas	2.73	2.65
Waste Management	1.59	0.73
Other Anthropogenic	0.39	0.51
Total Anthropogenic	*19.83*	*13.02*
Wetlands	–	12.54
Geological Seeps	–	0.28
Other Natural	–	0.25
Total Natural	–	*13.07*
– Total	**25.62**	

Figure 26. Estimate of Impact of Marcellus O&G activities on New York City Air Quality

The black line and shading show the mean ± 1 standard deviation in the EPA Air Quality System (AQS) maximum daily 8-hour average (MDA8) ozone for each monitoring site within the New York State–Northern New Jersey–Long Island, NY- NJ-CT Nonattainment Area. The red line and shading show the same for the GEOS-Chem model sampled at each monitoring site. The horizontal cyan line indicates the present NAAQS MDA8 ozone standard (70 ppbv). The horizontal green line indicates 1% of the present NAAQS MDA8 ozone standard. The blue line is the estimated contribution of Marcellus O&G emissions to MDA8, and at no point exceeds 0.7 ppbv during this period.

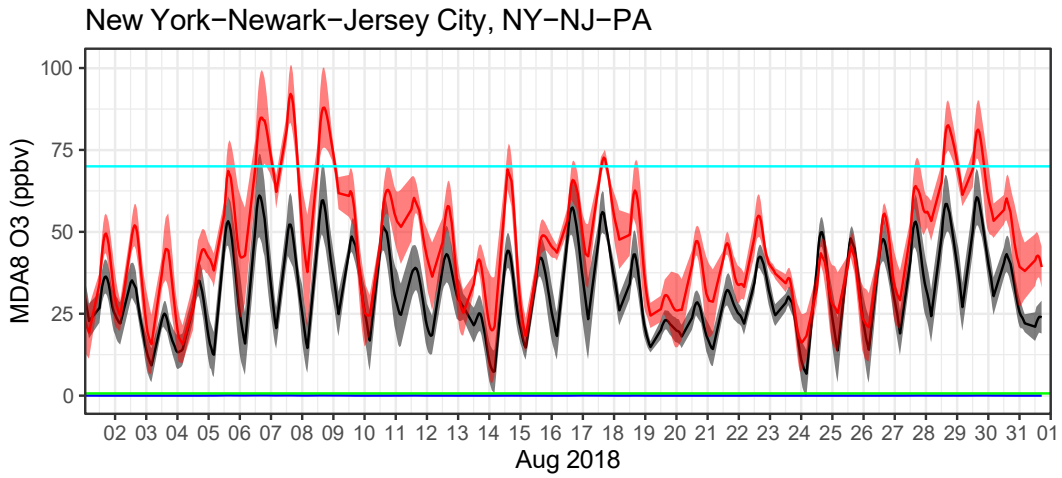

Previously, we explored the impact of fugitive emissions associated with O&G extraction in the Bakken Formation of North Dakota, but found no major population areas impacted (Kort et al., 2016). However, it raised the question as to what role fugitive NMVOC emissions from upwind O&G activities in the Marcellus region may have on downwind air quality, particularly in the New York–Northern New Jersey–Long Island, NY-NJ-CT Nonattainment Area.

Simulations were performed in which we prescribed Marcellus O&G methane from our optimized emissions and NMVOC emissions by using the well-pad ratios of NMVOC to methane from Swarthout et al. (2015) for ethane (C_2H_6), propane (C_3H_8), lumped C4+ alkanes, acetylene (C_2H_2), and benzene (C_6H_6). The model reasonably captures MDA8 for the month of August 2018. We then performed a sensitivity test in which we moved to the Marcellus VOC source to estimate the contribution on downwind air quality. At no point did the downwind impact on ozone exceed 0.7 ppbv at an urban area in the NEUS during a non-attainment event (see Figure 26).

Nevertheless, we plan to continue to explore the potential role of upwind emissions on downwind NEUS air quality as we continue refine our top-down constraints.

4 References

Bloom, A. A., K. W. Bowman, M. Lee, A. J. Turner, R. Schroeder, J. R. Worden, R. Weidner, K. C. McDonald, and D. J. Jacob (2017), A global wetland methane emissions and uncertainty dataset for atmospheric chemical transport models (WetCHARTs version 1.0), *Geoscientific Model Development*, *10*(6), 2141–2156, doi:10.5194/ gmd-10-2141-2017

Brasseur, G. P., and D. J. Jacob (2017), *Modeling of Atmospheric Chemistry*, Cambridge University Press, Cambridge.

Crippa, M., D. Guizzardi, M. Muntean, E. Schaaf, F. Dentener, J. A. van Aardenne,S. Monni, U. Doering, J. G. J. Olivier, V. Pagliari, and G. Janssens-Maenhout (2018), Gridded emissions of air pollutants for the period 1970–2012 within EDGAR v4.3.2, *Earth System Science Data*, *10*(4), 1987–2013, doi:10.5194/essd-10-1987-2018

Crosson, E. (2008), A cavity ring-down analyzer for measuring atmospheric levels of methane, carbon dioxide, and water vapor, *Applied Physics B*, *92*(3), 403–408, doi:10.1007/s00340-008-3135-y

Dlugokencky, E., E. Nisbet, R. Fisher, and D. Lowry (2011), Global atmospheric methane: budget, changes and dangers., *Philos Trans A Math Phys Eng Sci*, *369*(1943), 2058– 2072, doi:10.1098/rsta.2010.0341

EPA (2016), *Inventory of U.S. Greenhouse Gas Emissions and Sinks*: 1990-2014, EPA 430-R-16-002, 558 pp., Washington, DC.

Etheridge, D. M., L. P. Steele, R. J. Francey, and R. L. Langenfelds (1998), Atmospheric methane between 1000 A.D. and present: Evidence of anthropogenic emissions and climatic variability, *Journal of Geophysical Research: Atmospheres*, *103*(D13), 15,979– 15,993, doi:10.1029/98jd00923

Fiore, A., J. Oberman, M. Lin, L. Zhang, O. Clifton, D. Jacob, V. Naik, L. Horowitz, J. Pinto, and G. Milly (2014), Estimating North American background ozone in U.S. surface air with two independent global models: Variability, uncertainties, and recommendations, *Atmospheric Environment*, *96*, 284–300, doi:10.1016/j.atmosenv.2014.07.045

Fiore, A. M., J. J. West, L. W. Horowitz, V. Naik, and M. D. Schwarzkopf (2008), Characterizing the tropospheric ozone response to methane emission controls and the benefits to climate and air quality, *Journal of Geophysical Research*, *113*(D8), doi:10.1029/2007jd009162

Fung, I., J. John, J. Lerner, E. Matthews, M. Prather, L. P. Steele, and P. J. Fraser (1991), Three-dimensional model synthesis of the global methane cycle, *Journal of Geophysical Research*, *96*(D7), 13,033, doi:10.1029/91jd01247

Heald, C. L., D. J. Jacob, D. B. A. Jones, P. I. Palmer, J. A. Logan, D. G. Streets, G. W. Sachse, J. C. Gille, R. N. Hoffman, and T. Nehrkorn (2004), Comparative in- verse analysis of satellite (MOPITT) and aircraft (TRACE-P) observations to estimate Asian sources of carbon monoxide, *Journal of Geophysical Research: Atmospheres*, 109(D23), doi:10.1029/2004jd005185

Henze, D. K., A. Hakami, and J. H. Seinfeld (2007), Development of the adjoint of GEOS-Chem, *Atmospheric Chemistry and Physics*, *7* (9), 2413–2433, doi:10.5194/ acp-7-2413-2007

Hu, H., J. Landgraf, R. Detmers, T. Borsdorff, J. Aan de Brugh, I. Aben, A. Butz, and O. Hasekamp (2018), Toward Global Mapping of Methane With TROPOMI: First Results and Intersatellite Comparison to GOSAT, *Geophysical Research Letters*, *45*(8), 3682– 3689, doi:10.1002/2018gl077259

IPCC (2013), *Climate Change 2013: The Physical Science Basis. Contribution of Working Group I to the Fifth Assessment Report of the Intergovernmental Panel on Climate Change*, 1535 pp., Cambridge University Press, Cambridge, United Kingdom and New York, NY, USA.

Karion, A., W. Callahan, M. Stock, S. Prinzivalli, K. R. Verhulst, J. Kim, P. K. Salameh, I. Lopez-Coto, and J. Whetstone (2020), Greenhouse gas observations from the Northeast Corridor tower network, *Earth System Science Data*, *12*(1), 699–717, doi:10.5194/essd-12-699-2020

Kirschke, S., P. Bousquet, P. Ciais, M. Saunois, J. G. Canadell, E. J. Dlugokencky, P. Bergamaschi, D. Bergmann, D. R. Blake, L. Bruhwiler, P. Cameron-Smith, S. Castaldi, F. Chevallier, L. Feng, A. Fraser, M. Heimann, E. L. Hodson, S. Houweling, B. Josse, P. J. Fraser, P. B. Krummel, J.-F. Lamarque, R. L. Langenfelds, C. Le Quéré, V. Naik, S. O'Doherty, P. I. Palmer, I. Pison, D. Plummer, B. Poulter, R. G. Prinn, M. Rigby, B. Ringeval, M. Santini, M. Schmidt, D. T. Shindell, I. J. Simpson, R. Spahni, L. P. Steele, S. A. Strode, K. Sudo, S. Szopa, G. R. van der Werf, A. Voulgarakis, M. van Weele, R. F. Weiss, J. E. Williams, and G. Zeng (2013), Three decades of global methane sources and sinks, *Nature Geoscience*, *6*(10), 813–823, doi:10.1038/ngeo1955

Kort, E. A., M. L. Smith, L. T. Murray, A. Gvakharia, A. R. Brandt, J. Peischl, T. B. Ryerson, C. Sweeney, and K. Travis (2016), Fugitive emissions from the Bakken shale illustrate role of shale production in global ethane shift, *Geophysical Research Letters*, *43*(9), 4617–4623, doi:10.1002/2016gl068703

Loulergue, L., A. Schilt, R. Spahni, V. Masson-Delmotte, T. Blunier, B. Lemieux, J. Barnola, D. Raynaud, T. Stocker, and J. Chappellaz (2008), Orbital and millennial- scale features of atmospheric CH4 over the past 800,000 years., *Nature*, *453*(7193), 383–386, doi:10.1038/nature06950

Maasakkers, J., D. Jacob, M. Sulprizio, A. Turner, M. Weitz, T. Wirth, C. Hight, M. De- Figueiredo, M. Desai, R. Schmeltz, L. Hockstad, A. Bloom, K. Bowman, S. Jeong, and M. Fischer (2016), Gridded National Inventory of U.S. Methane Emissions., *Environ Sci Technol*, *50*(23), 13,123–13,133, doi:10.1021/acs.est.6b02878

Maasakkers, J. D., D. J. Jacob, M. P. Sulprizio, T. R. Scarpelli, H. Nesser, J.-X. Sheng, Y. Zhang, M. Hersher, A. A. Bloom, K. W. Bowman, J. R. Worden, G. Janssens- Maenhout, and R. J. Parker (2019), Global distribution of methane emissions, emis- sion trends, and OH concentrations and trends inferred from an inversion of GOSAT satellite data for 2010–2015, *Atmospheric Chemistry and Physics*, *19*(11), 7859–7881, doi:10.5194/acp-19-7859-2019

McKain, K. (2015), Atmospheric observations and models of greenhouse gas emissions in urban environments, Ph.D. thesis, Harvard University, Cambridge, MA.Miller, S., S. Wofsy, A. Michalak, E. Kort, A. Andrews, S. Biraud, E. Dlugokencky,J. Eluszkiewicz, M. Fischer, G. Janssens-Maenhout, B. Miller, J. Miller, S. Montzka, T. Nehrkorn, and C. Sweeney (2013), Anthropogenic emissions of methane in the United States, *Proc Natl Acad Sci U S A*, *110*(50), 20,018–20,022, doi:10.1073/pnas.1314392110

NYSDEC (2015), *Final Supplemental Generic Environmental Impact Statement on the Oil, Gas and Solution Mining Regulatory Program: Regulatory Program for Horizon- tal Drilling and High-Volume Hydraulic Fracturing to Develop the Marcellus Shale and Other Low-Permeability Gas Reservoirs*, 1448 pp.

NYSERDA (2019), *New York State Oil and Gas Sector Methane Emissions Inventory*: Final Report, Report Number 19-36, 196 pp.

NYSERDA, and NYSDEC (2019), New York State Greenhouse Gas Inventory: 1990– 2016, p. 73.

Prather, M. J., C. D. Holmes, and J. Hsu (2012), Reactive greenhouse gas scenarios: Systematic exploration of uncertainties and the role of atmospheric chemistry, *Geophysical Research Letters*, *39*(9), L09,803, doi:10.1029/2012gl051440

Pugliese, S. C., J. G. Murphy, F. R. Vogel, M. D. Moran, J. Zhang, Q. Zheng, C. A. Stroud, S. Ren, D. Worthy, and G. Broquet (2018), High-resolution quantification of atmospheric CO2 mixing ratios in the Greater Toronto Area, Canada, *Atmospheric Chemistry and Physics*, *18*(5), 3387–3401, doi:10.5194/acp-18-3387-2018

Saunois, M., P. Bousquet, B. Poulter, A. Peregon, P. Ciais, J. G. Canadell, E. J. Dlugo- kencky, G. Etiope, D. Bastviken, S. Houweling, G. Janssens-Maenhout, F. N. Tubiello,S. Castaldi, R. B. Jackson, M. Alexe, V. K. Arora, D. J. Beerling, P. Bergamaschi,D. R. Blake, G. Brailsford, V. Brovkin, L. Bruhwiler, C. Crevoisier, P. Crill, K. Covey,C. Curry, C. Frankenberg, N. Gedney, L. Höglund-Isaksson, M. Ishizawa, A. Ito, F. Joos, H.-S. Kim, T. Kleinen, P. Krummel, J.-F. Lamarque, R. Langenfelds, R. Locatelli,T. Machida, S. Maksyutov, K. C. McDonald, J. Marshall, J. R. Melton, I. Morino, V. Naik,S. O'Doherty, F.-J. W. Parmentier, P. K. Patra, C. Peng, S. Peng, G. P. Peters, I. Pison, C. Prigent, R. Prinn, M. Ramonet, W. J. Riley, M. Saito, M. Santini,R. Schroeder, I. J. Simpson, R. Spahni, P. Steele, A. Takizawa, B. F. Thornton, H. Tian,Y. Tohjima, N. Viovy, A. Voulgarakis, M. van Weele, G. R. van der Werf, R. Weiss,C. Wiedinmyer, D. J. Wilton, A. Wiltshire, D. Worthy, D. Wunch, X. Xu, Y. Yoshida,B. Zhang, Z. Zhang, and Q. Zhu (2016), The global methane budget 2000–2012, *Earth System Science Data*, *8*(2), 697–751, doi:10.5194/essd-8-697-2016

Sheng, J.-X., D. J. Jacob, J. D. Maasakkers, M. P. Sulprizio, D. Zavala-Araiza, and S. P. Hamburg (2017), A high-resolution (0.1? * 0.1?) inventory of methane emissions from Canadian and Mexican oil and gas systems, *Atmospheric Environment*, *158*, 211–215, doi:10.1016/j.atmosenv.2017.02.036

Swarthout, R. F., R. S. Russo, Y. Zhou, B. M. Miller, B. Mitchell, E. Horsman, E. Lipsky, D. C. McCabe, E. Baum, and B. C. Sive (2015), Impact of Marcellus Shale Natural Gas Development in Southwest Pennsylvania on Volatile Organic Compound Emissions and Regional Air Quality, *Environmental Science & Technology*, *49*(5), 3175–3184, doi:10.1021/es504315f

Thurston, G. D., and J. D. Spengler (1985), A quantitative assessment of source contributions to inhalable particulate matter pollution in metropolitan Boston, *Atmospheric Environment (1967)*, *19*(1), 9–25, doi:10.1016/0004-6981(85)90132-5

Turner, A. J., D. J. Jacob, K. J. Wecht, J. D. Maasakkers, E. Lundgren, A. E. Andrews, S. C. Biraud, H. Boesch, K. W. Bowman, N. M. Deutscher, M. K. Dubey, D. W. T. Grif- fith, F. Hase, A. Kuze, J. Notholt, H. Ohyama, R. Parker, V. H. Payne, R. Sussmann, C. Sweeney, V. A. Velazco, T. Warneke, P. O. Wennberg, and D. Wunch (2015), Es- timating global and North American methane emissions with high spatial resolution using GOSAT satellite data, *Atmospheric Chemistry and Physics*, 15(12), 7049–7069, doi:10.5194/acp-15-7049-2015

Turner, A. J., D. J. Jacob, J. Benmergui, S. C. Wofsy, J. D. Maasakkers, A. Butz, O. Hasekamp, and S. C. Biraud (2016), A large increase in U.S. methane emissions over the past decade inferred from satellite data and surface observations, *Geophysical Research Letters*, *43*(5), 2218–2224, doi:10.1002/2016gl067987

Wecht, K. J., D. J. Jacob, C. Frankenberg, Z. Jiang, and D. R. Blake (2014), Mapping of North American methane emissions with high spatial resolution by inversion of SCIAMACHY satellite data, *Journal of Geophysical Research: Atmospheres*, *119*(12), 7741– 7756, doi:10.1002/2014jd021551

WMO, and UNEP (2011), *Integrated Assessment of Black Carbon and Tropospheric Ozone: Summary for Decision Makers*, WMO - No. 1073, 285 pp., UNON/Publishing Services Section, Nairobi.

Zhang, L., D. J. Jacob, N. V. Downey, D. A. Wood, D. Blewitt, C. C. Carouge, A. van Donkelaar, D. B. A. Jones, L. T. Murray, and Y. Wang (2011), Improved estimate of the policy-relevant background ozone in the United States using the GEOS-Chem global model with 1/2º x 2/3º horizontal resolution over North America, *Atmospheric Environment*, *45*(37), 6769–6776, doi:10.1016/j.atmosenv.2011.07.054

Endnotes

[1] University of Rochester Atmospheric Chemistry and Climate Group; http://atmos.earth.rochester.edu

[2] GEOS-Chem Model Website; http://www.geos-chem.org

[3] GEOS-Chem Model Public Repository; https://github.com/geoschem/geos-chem

[4] GEOS-Chem ComputeCanada Input Data Repository; http://geoschemdata.computecanada.ca

[5] GEOS-Chem Adjoint Website: http://adjoint.colorado.edu

[6] ACT-America Campaign Website; https://act-america.larc.nasa.gov

[7] NOAA Global Monitoring Laboratory Trends; https://www.esrl.noaa.gov/gmd/ccgg/trends/gl_gr.html

NYSERDA, a public benefit corporation, offers objective information and analysis, innovative programs, technical expertise, and support to help New Yorkers increase energy efficiency, save money, use renewable energy, and reduce reliance on fossil fuels. NYSERDA professionals work to protect the environment and create clean-energy jobs. NYSERDA has been developing partnerships to advance innovative energy solutions in New York State since 1975.

To learn more about NYSERDA's programs and funding opportunities, visit nyserda.ny.gov or follow us on Twitter, Facebook, YouTube, or Instagram.

New York State Energy Research and Development Authority

17 Columbia Circle
Albany, NY 12203-6399

toll free: 866-NYSERDA
local: 518-862-1090
fax: 518-862-1091

info@nyserda.ny.gov
nyserda.ny.gov

State of New York
Kathy Hochul, Governor

New York State Energy Research and Development Authority
Richard L. Kauffman, Chair | Doreen M. Harris, President and CEO